Bidirectional River-Floodplain Connectivity During Combined Pluvial-Fluvial Events

Nelson Tull[1], Paola Passalacqua[1], Hima J. Hassenruck-Gudipati[2], Shazzadur Rahman[1*], Kyle Wright[1], Jayaram Hariharan[1], and David Mohrig[2]

[1]Department of Civil, Architectural and Environmental Engineering, Center for Water and the Environment, University of Texas at Austin, Austin, TX, USA
[2]Department of Geosciences, Jackson School of Geosciences, University of Texas at Austin, Austin, TX, USA

Key Points:

- Field data and modeling show distinct signals of pluvial and fluvial flooding
- Floodplain residence times change dramatically between pluvial and fluvial phases of the storm
- Flows between river and floodplain are dominated by the largest channels and levee depressions

*Walter P. Moore, Houston, TX

Corresponding author: Paola Passalacqua, paola@austin.utexas.edu

Abstract

Hydrologic connectivity controls the lateral exchange of water, solids, and solutes between rivers and floodplains, and is critical to ecosystem function, water treatment, flood attenuation, and geomorphic processes. This connectivity has been well-studied, typically through the lens of fluvial flooding. In regions prone to heavy rainfall, the timing and magnitude of lateral exchange may be altered by pluvial flooding on the floodplain. We collected measurements of flow depth and velocity in the Trinity River floodplain in coastal Texas (USA) during Tropical Storm Imelda (2019), which produced up to 75 cm of rainfall locally. We developed a two-dimensional hydrodynamic model at high resolution for a section of the Trinity River floodplain inspired by the compound flooding of Imelda. We then employed Lagrangian particle routing to quantify how residence times and particle velocities changed as flooding shifted from rainfall-driven to river-driven. Our results show that heavy rainfall initiated lateral exchange before river discharge reached flood levels. The presence of rainwater also reduced floodplain storage, causing river water to be confined to a narrow corridor on the floodplain, while rainwater residence times were increased from the effect of high river flow. Finally, we analyzed the role of floodplain channels in facilitating hydrologic connectivity by varying model resolution in the floodplain. While the resolution of floodplain channels was important locally, it did not affect as much the overall floodplain behavior. This study demonstrates the complexity of floodplain hydrodynamics under conditions of heavy rainfall, with implications for sediment deposition and nutrient removal during floods.

Plain Language Summary

Unaltered river floodplains can support diverse ecosystems, reduce flooding, and remove nutrients from river water. Floodplains near the coast are particularly important, as they typically experience more frequent flooding. Floodplain function relies on a high degree of connectivity with the river, where water can move easily through the floodplain during periods of high river stage. Our study explores the ways in which heavy rainfall on a floodplain impacts this connectivity. We collected flow measurements in the Trinity River floodplain (Texas, USA) during Tropical Storm Imelda in 2019 that showed distinct flooding patterns between the rainfall and river flooding. We coupled a hydrodynamic model with a particle tracking module to see how particles in the water might move through the floodplain during the transition from rainfall-driven to river-driven flooding. We found that the average time a particle spent in the floodplain changed significantly after the rain in the model stopped. We also noticed that rainwater tended to remain in the floodplain for much longer than river water, especially after the rain stopped. This study describes the various interactions that can occur between local rainfall and river flooding, and moves toward a better understanding of sediment and nutrient transport through floodplains.

1 Introduction

River floodplains play a fundamental role in flood storage, nutrient cycling, sediment retention, and in general provide support for diverse ecosystems (Ward et al., 1999; Melack & Forsberg, 2001; Kondolf et al., 2006; Roley et al., 2012; Noe et al., 2013; Kufel & Leśniczuk, 2014). Floodplains are complex and heterogeneous, and their structure and function are highly dependent on their degree of connectivity with the river (Hughes et al., 2001; Harvey & Gooseff, 2015; Gurnell et al., 2016; Covino, 2017). Topographic controls on hydrologic connectivity, defined here as the degree of surface water movement between rivers and floodplains, have been described for the largest river-floodplain systems using satellite imagery (Lesack & Melack, 1995; Mertes et al., 1995; Mertes, 1997; Alsdorf et al., 2007; Trigg et al., 2012; Lewin & Ashworth, 2014; Park & Latrubesse, 2017), and more recently for medium-size rivers using lidar data and numerical modeling (David et al., 2017; Czuba et al., 2019; Byrne et al., 2019). However, river-floodplain connectivity is poorly understood when hydrodynamics are partially driven by local rainfall. Mixing of

rainfall and river floodwaters has been observed and discussed for very large river floodplains (Mertes, 1997; Alsdorf et al., 2007; Day et al., 2008; Rowland et al., 2009; Trigg et al., 2012), where floodplain channels are at a large enough scale to be sensed remotely, and the flood wave occurs over much longer time scales (Junk et al., 1989). But for medium-size rivers, flood waves are less predictable, and floodplain features are often too small to detect using satellite imagery. The goals of this study are to show (a) the impact of local rainfall on floodplain residence times, flow directions, and connectivity within the floodplain, and (b) to determine the role of floodplain channels in facilitating river-floodplain exchange under combined pluvial-fluvial flooding conditions.

Floodplain topography has been shown as a key control on mixing of local runoff and river waters in large floodplain systems, where most mixing tends to occur outside of channel features (Lesack & Melack, 1995; Mertes et al., 1995; Mertes, 1997; Trigg et al., 2012). Flow within floodplain channels can be bidirectional due to the advancing and receding of the flood wave and the timing of rainfall runoff on the floodplain (Alsdorf et al., 2007; Day et al., 2008; Rowland et al., 2009). For smaller river systems as well, sub-bankfull discharges can result in floodplain inundation that is limited spatially by the extent of lateral floodplain channels in the system (Kupfer et al., 2015; Czuba et al., 2019). Pluvial flooding may enhance hydrologic connectivity within the floodplain by bringing inundation, and potentially nutrients and sediment, to areas of the floodplain that would otherwise be out of reach for river waters. On the other hand, if intense enough, pluvial flooding can develop a water surface gradient moving from floodplain to channel, which may reduce flux into the floodplain (Day et al., 2008). It is common that fluvial and pluvial flooding at a site are not coincident in time, as a result of a storm moving slowly over a watershed, and thus the interaction between the two flooding modes may be complex in space and time. Recent studies of river-floodplain connectivity have used unsteady numerical models to show how floodplain hydrodynamics evolve with the rising and falling of a river flood wave (Byrne et al., 2019; Chen et al., 2020), but no study has used numerical modeling to analyze the interaction of fluvial and pluvial flooding. Furthermore, no study to-date has presented field measurements of floodplain flow that differentiate these two flooding modes.

The interaction of pluvial and fluvial flooding may have significant impacts on residence time, flow direction, and the overall extent of hydrologic connectivity in river-floodplain systems, all of which can be drivers of dissolved nutrient sequestration (Mann & Wetzel, 1995; Tockner et al., 1999; Aufdenkampe et al., 2011; Noe & Hupp, 2005; Noe et al., 2013; Wolf et al., 2013; Cheng & Basu, 2017) and sediment deposition (Tockner et al., 1999; Verhoeven et al., 2001; Schulz et al., 2003; Day et al., 2008; Trigg et al., 2012; Juez et al., 2019) in floodplains. Sediment deposition depends on local availability from the river, as well as flow velocity distributions across the floodplain to advect the sediment (Marriott, 1992; Asselman & Middelkoop, 1995), while dissolved nutrients require sufficient contact time to be removed from floodwaters via biogeochemical processes (Tockner et al., 1999; Noe et al., 2013; Cheng & Basu, 2017). The depositional environments of lowland river floodplains are understood to provide conditions conducive to these processes, yet it is unknown how conditions change when pluvial flooding is substantial.

In this study we show how pluvial flooding impacts residence time distributions and flow patterns in a low-gradient river-floodplain system by using the lower Trinity River (Texas, USA) as a study site. To our knowledge this is the first modeling study of pluvial flooding in the context of hydrologic connectivity. We present flow depth and velocity measurements collected during Tropical Storm Imelda (2019) in the Trinity River floodplain that show clear and separate signals of pluvial and fluvial flooding. We then develop a two-dimensional, depth-averaged numerical model with high mesh resolution inspired by the observed hydrodynamics during the storm. Next, we employ a Lagrangian particle routing tool on the unsteady model flow field to quantify how rainfall and channel processes impact residence time distributions and flow patterns in floodplains. Lastly, we perform a model

resolution scaling analysis to determine how flux to and from the floodplain changes as floodplain channels are smoothed out of the model.

The outline of the manuscript is as follows. Section 2 describes the characteristics of the lower Trinity River study site, including a description of the elevation data used for this study. Section 3 introduces Tropical Storm Imelda, the test-case event, and the hydrodynamic data collected in the Trinity River floodplain in 2019 during the storm. Section 4 introduces the ANUGA (Eulerian) and *dorado* (Lagrangian) models, and describes the modeling approach. Section 5 presents the results of the study, including the unique impacts of rainfall on floodplain hydrodynamics. Section 6 provides a discussion of implications for floodplain services and for future modeling studies of river-floodplain connectivity. Lastly, Section 7 summarizes the major findings of the study.

2 Study Area: The Trinity River

2.1 Site Description

The Trinity River basin ($40,000$ km^2) extends from its outlet in Trinity Bay into north-central Texas (Figure 1A). The area of investigation spans about 10.5 river kilometers (rkm) of the lower basin in Liberty County, between Liberty and Wallisville, TX. The study area is within the river's backwater reach (BWR), which is recognized by the asymptotic approach of the water surface elevation to the surface elevation of the receiving basin. Under low-discharge conditions, the BWR begins approximately 15 rkm upstream of the study area (Figure 1B) (Mason & Mohrig, 2018).

As the river transitions from a normal flow regime to the BWR, the channel morphodynamics respond to the adjustments in flow conditions and the transport of solids. This transition coincides with downstream narrowing and deepening of the channel. Rates of channel-bend migration decrease in the downstream direction, as do the size and shape of point bars, and grain size of bed material (Smith et al., 2020). Similarly, the overbank conditions vary in accordance with the transition to the BWR. For example, upstream of the BWR, the floodplain is geomorphically active (Mason & Mohrig, 2018; Hassenruck-Gudipati, 2021) and it largely remains dry during low and moderate flow conditions, but is inundated during floods, when water emerges from channel confinement and spreads across the floodplain. In contrast, the BWR is characterized by a wetland environment due to its relatively low elevation and is prone to inundation by moderate river discharges. Stage change between low and flood flows is smaller in the BWR, with lateral flow spreading playing a greater role due to the low-gradient environment and reduced freeboard between normal flow water surface elevation and the adjacent floodplains (Smith et al., 2020). Because of these characteristics, surface-water connectivity is greater in the study reach compared to upstream reaches, and floodplain channels are more commonplace and pronounced. This connectivity may cause a degree of "leakiness" in the system, which would be supported by the large decrease in average annual peak discharge between Liberty ($2,477$ m^3/s, USGS 08067000) and Wallisville (756 m^3/s, USGS 08067252) (see Figure 1B for locations).

Like many fluvial-deltaic systems worldwide, the Trinity is not free of anthropogenic influences. Within the study area (Figure 1C), there is a single, raised access pathway that traverses the river-right floodplain perpendicular to the main flow direction. The pathway contains several bridges and culverts that pass flow through the larger floodplain channels. Also in the study area are three buried pipeline rights-of-way that are cleared of trees, and currently consist of very tall grasses and shrubs. Just upstream of the study area but within the connected floodplain is another old, raised pathway along a levee that has been eroded significantly due to lack of use and maintenance. Upstream of the study area but south of Liberty, the floodplain contains remnants of oil drilling operations, although this part of the floodplain is disconnected hydraulically from the current study area due to a natural pinch-point along the right bank of the river. There are also two water diversion operations

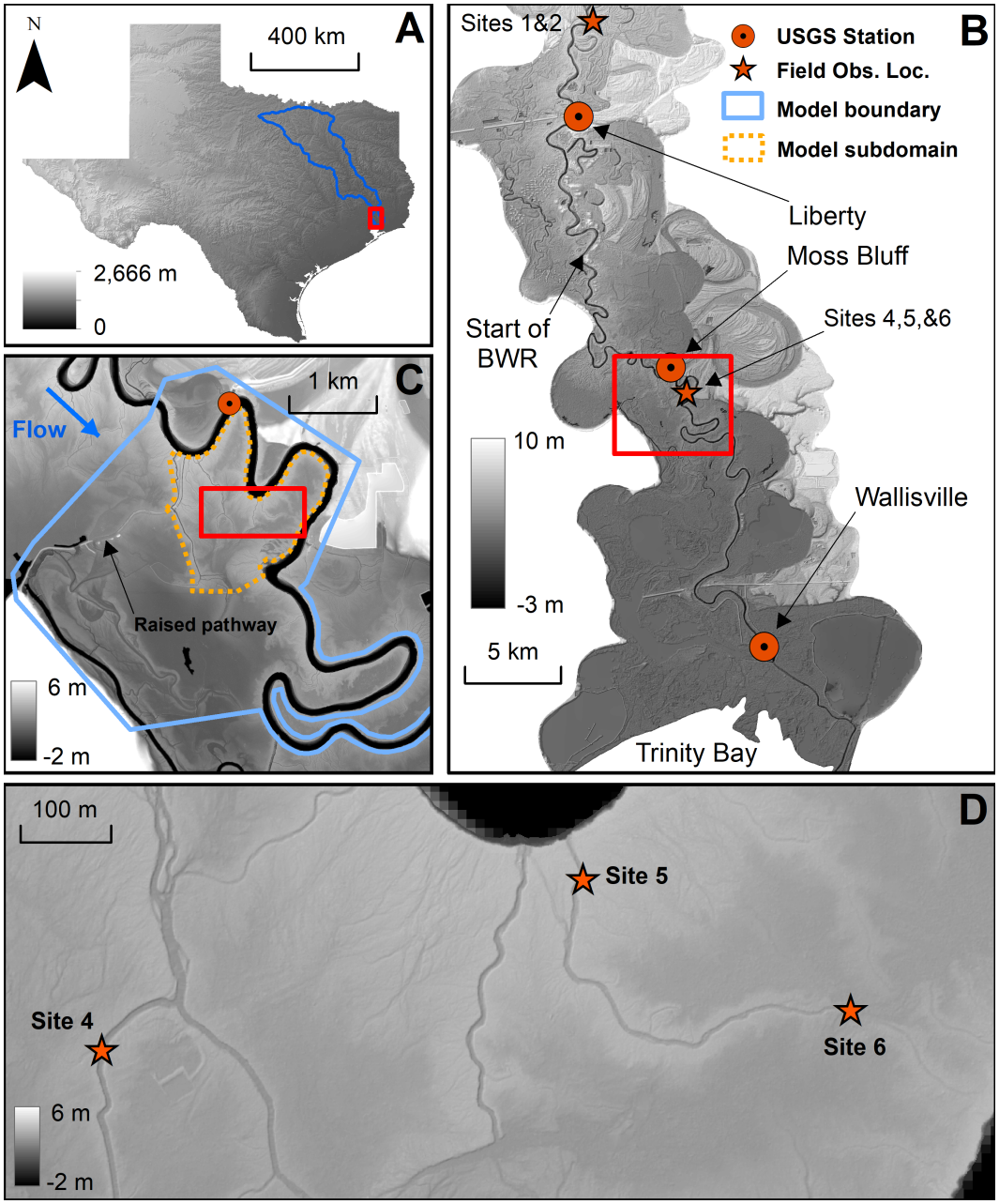

Figure 1. Elevation maps of the Trinity River study area. (A) Location of the Trinity River basin in Texas. (B) Lidar DEM for Trinity River floodplains between Liberty (upstream) and Wallisville (downstream), including locations of field observation sites. (C) Boundary of model domain used in this study. The yellow dashed boundary represents the area in our models with higher mesh resolution. The downstream boundary of the model domain extends to Wallisville, but is not shown here. (D) Location of field sites in the floodplain. Sites 4 and 5 are within channels, while Site 6 is just outside a channel terminus in a floodplain basin.

in the area, both of which are located on perched topography above the floodplain. Perhaps most notably, the Livingston Dam (far upstream of the study area) is a run-of-river dam that impacts the river geomorphology for the first 50-60 rkm downstream of the structure

(Phillips et al., 2004; Phillips & Slattery, 2007; Smith & Mohrig, 2017). Beyond this point, sediment mining from the bed and banks of the river re-establishes the bed-material load (Smith & Mohrig, 2017) and no changes in channel geometry and kinematics have been observed since reservoir filling. Despite these various human influences, the study reach is unaffected by significant modifications such as containment levees, wing dykes, and revetments; thus, the river is able to operate unhindered within its valley.

We chose the model domain boundary (Figure 1C) for three main reasons. First, the domain contains three of the field observation sites (see Section 3.2) that recorded data during Tropical Storm Imelda. Second, and related to the first, the floodplain topography in this area features many channels of various sizes that connect the river to the floodplain (Figure 1D). Floodplain channel widths range from small, 1-2 m channels barely detectable in the lidar, to larger, 8-10 m channels with greater depths that most likely play a larger role in river-floodplain exchange. The complex floodplain topography makes this location interesting to study. Third, the domain boundary needed to be limited in space, as the high-resolution modeling needed to resolve the smallest channels requires significant computational resources.

2.2 Elevation Data

All elevation data and references to elevation in this manuscript are relative to the NAVD88 datum. The elevation data shown in Figure 1 were derived from lidar measurements collected in February and March of 2017 as part of the Texas Strategic Mapping Program. Data were acquired and processed by the Sanborn Map Company with third party quality assurance and control provided by AECOM. Collection took place during the leaf-off season in Texas. The reported horizontal and vertical accuracy of the lidar are 0.25 and 0.29 m, respectively.

The lidar data were interpolated to a bare-earth digital elevation model (DEM) at 1-m resolution. Small voids in the floodplain lidar were interpolated using a second-degree polygon plane fit through the existing data. For larger voids corresponding to floodplain ponds, major channels, and oxbows, bathymetry was approximated by performing the same plane fitting interpolation as above, followed by a 5-m downward shift of the elevation. River bathymetry measurements were taken by the Trinity River Authority in 2017, along four longitudinal profiles at transects spaced every 400 m on average (the river width varies between 80 and 100 m). The bathymetry was interpolated to a 10-m grid, and patched together with the lidar DEM using the Raster to Mosaic tool in ArcGIS. Finally, linear interpolation was performed across the small gaps between the lidar DEM and bathymetry raster.

3 Tropical Storm Imelda

3.1 Storm Background

Tropical Storm Imelda (2019) was a major rainfall event that produced over 75 cm of precipitation across several counties in the area surrounding Houston, TX (Latto & Berg, 2020). Imelda made landfall near Freeport, TX (120 km southwest of the study site) on 17 September 2019 as a tropical storm, before quickly weakening to a tropical depression as it moved slowly northward through Houston, TX and subsequently across the lower Trinity River watershed. The storm further degenerated to a trough by 19 September, at approximately 160 km north-northeast of Houston, where it continued to dissipate and move northward. The highest recorded rainfall total from Imelda was 112 cm over a three-day period near Fannett, TX, with 79 cm falling within a 31-hour period, which made it the fifth wettest tropical cyclone ever recorded in the contiguous United States.

Eastern Texas experienced widespread pluvial flooding during this period. While the lower Trinity River watershed received much of this rainfall, including up to 75 cm at the study site, the river stage at the Liberty USGS station peaked just below the official flood stage on 20 September as defined by the National Weather Service. Likewise, at the Moss Bluff USGS station downstream, the peak stage of 4.0 m was below the adjacent levee crests but over a meter above many of the nearby floodplain channel bottom elevations in the DEM. A sub-bankfull flood event is suitable for analyzing river-floodplain connectivity, as floodplain channels are activated and responsible for any lateral exchange that occurs, and floodplain inundation is heterogeneous (Czuba et al., 2019). The timing mismatch of the pluvial and fluvial flooding peaks, along with the sheer volume of precipitation, created an opportunity for competition between river and floodplain water worth investigating.

3.2 Field Data Collection

During August 2019, six outdoor trail cameras, six measuring rods, six water level loggers (Solinst Levelogger, Model 3001), and four tilt current meters (TCM-1 from Lowell Instruments) were installed at various floodplain locations along the Trinity River (Figure 1). The loggers recorded water level every six minutes, while the tilt current meters recorded flow speed and direction every minute. The cameras took a photograph of the installation plus measuring rod every five minutes, night and day. The instruments were left in the field until February 2020, and successfully collected data during Tropical Storm Imelda. Sites 1, 2, and 3 were located north of Liberty near the bend indicated in Figure 1B (plan view of exact locations of Sites 1 and 2 is shown in Supporting Information Figure S1). Site 1, located in a large floodplain channel, collected water level velocity readings, while Site 2, located in a shallow levee-traversing channel, collected water levels only. Instruments at Site 3 were displaced and lost during the storm. Sites 4, 5, and 6 were all located in the study area (Figure 1C and D). Sites 4 and 6 collected both water level and velocity readings, while Site 5 collected water levels only. Site 4 instruments were located in a floodplain channel roughly 930 m from the Trinity River (measured along the channel). Site 5 was located on a different floodplain channel, just 50 m from the river and higher on the river levee. The floodplain slopes downward away from the river, with Sites 4 and 6 at lower elevations than Site 5. Site 6 was located at the terminus of the same channel monitored by Site 5. At Site 6 a small internal delta is building out from the mouth of the floodplain channel into the adjacent, small floodplain basin with perennial standing water. Sites 5 and 6 were located on a channel connected to the river bend just downstream from the USGS station at Moss Bluff, while the Site 4 floodplain channel connected to the river immediately upstream of Moss Bluff (Figure 1). The field instrument locations provided a diverse set of topographic and hydrologic conditions for observing the patterns of rainfall and river flooding that occurred during Imelda.

Water level and velocity measurements collected during Imelda provided a depiction of hydrodynamics in the floodplain (Figure 2). Each set of water level logger measurements showed a clear distinction between floodplain inundation due to rain (hours 24–72, counting from the start of 17 September 2019) and inundation due to rising river stage (hours 72–144, Figure 2A). Since the precipitation was centered over the site, the floodplain response to precipitation always preceded that tied to river stage. Still, flooding patterns varied depending on specifics of the monitored location. During the early hours of 19 September (hour 48), the floodplain channel at Site 5 saw water levels rise and fall with each sequential rain band before the river WSE had risen to the elevation of that channel. Later that day, the river stage had risen to an elevation of 3.17 m, corresponding to the elevation at which river water contributed to flow in the floodplain channel. As Site 5 was located only 50 m from the river bank, the peak flow depth at this location tracked river stage closely until the stage fell below the floodplain channel elevation. Water level fluctuations at the Site 4 floodplain channel were similar to Site 5, but the 80 cm increase in water levels during the rainfall phase was more substantial than the increase at Site 5, likely due to the larger catchment area of Site 4. River stage reached the elevation of the Site 4 channel at an

elevation of 2.95 m. Peak water levels at Site 4 also corresponded to peak river stage, although the rate of drainage during the falling limb was different from those at Site 5 and the main channel, which is also likely related to the longer distance between Site 4 and the river. At Site 6, water level data showed a signal of both rainfall and river flooding, albeit less pronounced than the channelized locations of Sites 4 and 5. Farther upstream, data from Site 2 on a high levee showed a fast increase in water levels during peak rainfall as its local floodplain basin filled up, but unlike the downstream sites, there was no signal of river flooding. In this case, river stage was insufficient to overtop the levee.

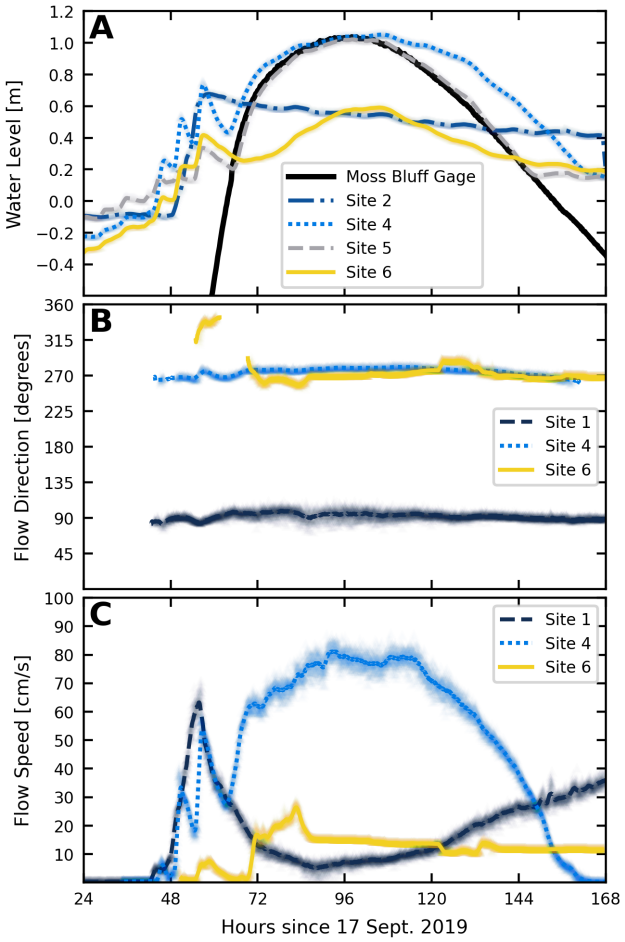

Figure 2. Flow patterns observed in field data in the Trinity River floodplain during Tropical Storm Imelda. Lines represent moving averages of the data, while the raw data are shown underneath in very light colors. (A) Measured water level fluctuations, compared to river water levels at the nearby USGS gage. Note the USGS gage data here are relative, having been translated vertically to show the similar rates of water level change between the river and the Site 5 channel. Also note measured water levels are plotted relative to the initial recorded depths at each site, see Supporting Information Dataset S1 for more information. (B) Flow direction histories for three floodplain channels. Data are oriented so that 90 degrees aligns with flow out of channel and into river, and 270 degrees aligns with flow out of river and into floodplain. Flow directions are only plotted for velocities exceeding 5 cm/s and logger depth recordings exceeding 76 cm (based on instrument specifications). (C) Velocity histories at Sites 1, 4, and 6.

Velocity measurements showed diverse flow patterns. At Site 1, water in the floodplain channel flowed out to the river throughout the entire event, with peak velocity tied to peak rainfall, not river stage (Figure 2B and C). Velocities were lower at Site 6 because it is an unchannelized location, situated at the transition between the mouth of a floodplain channel and its connected, small floodplain basin. Interestingly, peak velocity at Site 6 occurred during the period when pluvial flooding drained but prior to arrival of peak river stage. Less than 1 km away in the Site 4 floodplain channel farther from the river, water always flowed away from the river into the floodplain interior (Figure 2B and C). Imagery collected by the time-lapse cameras confirmed these observations, showing a rapid rise in water level soon after the beginning of rainfall, followed by a pattern of drainage consistent with saturated soil conditions throughout the event. The field data collected during the storm showed several distinct patterns of pluvial and fluvial flooding, and provide the inspiration for the modeling efforts in this study.

It is important to contextualize these observations with instrument limitations. The water level logger measurements are relative; that is, they are not tied to any datum. During a storm event, it is also possible for loggers to become buried with sediment, and for floodplain geometry to change significantly (Mason & Mohrig, 2018; Hassenruck-Gudipati, 2021). For these reasons, it is uncertain how the water levels measured in 2019 relate to elevations and floodplain geometry in the 2017 lidar dataset described in Section 2.2 and used for the modeling in this study. Additionally, the tilt current meters are typically used for deeper-water applications, and have a minimum required depth for accurate results (Lowell et al., 2015). The study of water in floodplains, particularly in the absence of total inundation, involves relatively shallow environments. Therefore, we only present velocity data that meet the minimum depth criterion of 76 cm.

4 Modeling Approach

We employed a numerical model and a Lagrangian particle routing tool to analyze the hydrodynamics of the Trinity River floodplain during Tropical Storm Imelda. First, a numerical model with high-resolution in the floodplain area of interest was developed for the study reach. Simulation results were compared to field measurements of depth in the floodplain. The simulation flow field was used to model passive particle transport and compute average particle speeds and residence times across the floodplain. A set of additional numerical models was then developed for the same domain, each with progressively lower resolution in the floodplain, and lateral flux was computed and compared between models. Through these methods, we infer the relative impact of pluvial and fluvial flooding, as well as the role of floodplain channel topography, on floodplain hydrodynamics.

4.1 ANUGA Model Development

We use the ANUGA hydrodynamic model for numerical modeling in this study. ANUGA is an open-source model developed by researchers at the Australian National University and Geoscience Australia (Roberts et al., 2015). It solves the shallow-water equations using unstructured meshes and a finite-volume numerical scheme. Details of the numerical scheme can be found in Nielsen et al. (2005), Mungkasi and Roberts (2011), and Mungkasi and Roberts (2013). ANUGA is the model of choice for several reasons, including: (*i*) it is open-source and therefore easy to control and customize; (*ii*) the finite-volume method conserves mass and momentum along the wetting-drying front; (*iii*) it uses unstructured meshes; (*iv*) it scales efficiently in high performance computing environments; and (*v*) it employs a variable time step. The flexibility of the unstructured mesh allows for higher model resolution in areas of higher priority, while offering reduced resolution in areas of less concern. This, along with the parallel capabilities and variable time step, reduces the computational resources needed for model simulations, which is important for an application where near-lidar-scale mesh resolution was used.

The model domain boundary (shown in Figure 1C) was delineated to incorporate all channel and overbank areas contributing flow to the floodplain area of interest, while using the smallest domain possible for computational reasons. The majority of the model domain consisted of an unstructured mesh with a constant average element edge length of 20 m. The 20 m element size is approximately one-fifth of the width of the main channel, which provided a sufficient representation of the channel cross-section geometry. Twenty-m resolution was too coarse to resolve most floodplain channels along the Trinity, and was only able to resolve longer-range elevation changes, such as a floodplain basin or a group of nearby floodplain channels that are averaged collectively into a smooth low area. Within the floodplain region surrounding the three field sites (dashed yellow boundary in Figure 1C), the mesh resolution was increased to 2 m, resulting in a total of 1,308,101 mesh elements. At this resolution, nearly all of the floodplain channels are resolved. The constant, 2-m resolution boundary extends to the edge of the channel, where it transitions to the background spacing of 20 m. As a result, elements in the channel adjacent to the high-resolution boundary are finer than elsewhere in the domain where the general spacing is 20 m.

The upstream, left floodplain, and right floodplain boundaries were modeled as no-flow (reflective) boundaries. The downstream domain boundary extended approximately 13.4 rkm from the study site to Wallisville, TX. This extension included only the river channel itself, and was appended to the domain to provide a sufficient distance between the study site and the downstream river boundary condition. A constant water surface elevation (WSE) of 0.7 m (NAVD88) was imposed at the downstream boundary, representing the mean WSE measured at the Wallisville USGS station over a 10-day period preceding the storm. We found the model to be insensitive to this boundary condition. The longitudinal boundaries along the channel levees of this extension were modeled as transmissive boundaries to allow for any overbank flow to pass out of the domain. The boundary traversing the river-right floodplain at the downstream end was modeled as a quasi-transmissive boundary. This was a time-varying, zero-momentum boundary with a WSE always equal to 5 cm below the current WSE in the domain adjacent to the boundary. This boundary condition was used as an approximation to the water surface slope moving through the floodplain.

The DEM described in Section 2.2 was applied to mesh vertices via a least-squares fit with minimal smoothing. Elevations at mesh element centroids were computed as the average of the three vertices, creating a discontinuous, piecewise-constant elevation surface used by the ANUGA "DE1" flow algorithm (Davies & Roberts, 2015). Friction forcing was applied to the domain as two constant Manning's n values: 0.025 within the main channel and 0.075 in the floodplain. These values were chosen based on guidance from literature (Chow, 1959) and judgment from field visits and site photographs. River floodplains are clearly heterogeneous, with dense forested areas expected to have a higher flow resistance than the channelized portions that are a focus of this study. Although n values are typically suggested at or just over 0.1 for forested areas, we applied the lower value of 0.075 as a compromise between the hydraulic characteristics of channelized and forested areas.

The model was run over an 8-day period, beginning at 0000 Central Time on 17 September 2019 and lasting through 24 September. The model was forced using a calibrated hydrograph based on discharge data from the Liberty USGS station. The base flow recorded at Liberty at the starting time was 52 m^3/s, while the peak discharge from Imelda was 793 m^3/s, occurring at 1100 on 21 September. The Liberty USGS station hydrograph was calibrated to match the observed WSE in the channel at Moss Bluff (USGS 08067100) where there is no available hydrograph, as it is unknown how much the event discharge changes from Liberty to Moss Bluff. To develop a hydrograph for the model domain, several model simulations were run using the Liberty station as a starting point. With each subsequent simulation, the model stage was compared with the observed stage at Moss Bluff, and the model discharge was adjusted from the previous by the same ratio as the difference in modeled and observed stage. This linear calibration results in a near-perfect match between modeled and observed water levels at Moss Bluff. The calibrated hydrograph used to force

the model has an initial discharge of 32 m^3/s and a peak discharge of 681 m^3/s (Figure 3). Similar to USGS data in general, discharge values were generated in 15-minute intervals, and these values were applied to the model at each time step using linear interpolation between intervals (see Dataset S2 for the full calibrated hydrograph). This procedure provides the most direct way to force water surface gradients between the river and floodplain to be as close as possible to those observed by the local river gage.

Rainfall data from Imelda in 15-minute intervals were retrieved from the Liberty USGS station, which posts data for a period of 120 days after the storm. These data were not official or quality assured, but the timing and depths of peak rainfall were similar to those reported elsewhere. The data consisted of three distinct passovers of tropical storm bands, corresponding to large hyetograph bars (Figure 3) and spikes in water levels observed on the floodplain (Figure 2A). The data show the first rainfall band arriving at hour 45 (2100 CT, 18 September) and the third band ending at hour 63.5. The combined depth of rainfall added to the model from the three bands was 75.3 cm. This depth corresponds to a total volume of 1.0×10^6 m^3 added to the domain over an 18.5-hour period. A less intense, background rainfall rate was also added to the model to replicate the steady accumulation of water observed in the field data prior to arrival of the high-intensity tropical storm bands (see Datasets S3 and S4 for the raw and modified hyetograph applied to the model). Rainfall was applied evenly across the entire domain as depths per second. Runoff from outside of the model domain was not considered in this study.

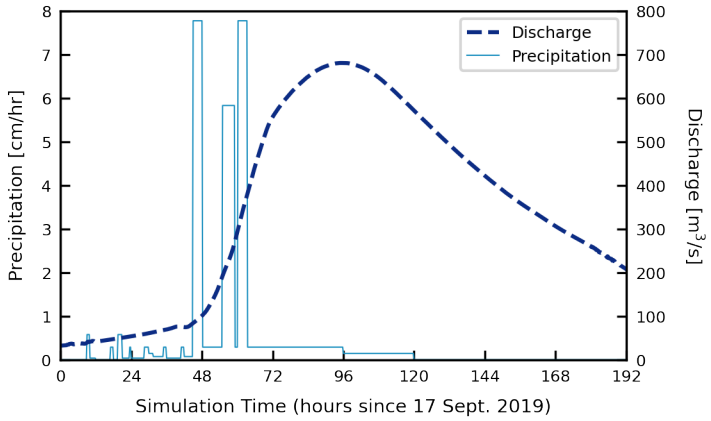

Figure 3. Hydrograph and hyetograph for Tropical Storm Imelda as applied to the numerical model.

4.2 Quantifying Residence Times with *dorado*

dorado (Hariharan et al., 2020) is an open-source, Lagrangian particle routing package that uses a D-8 random walk algorithm (Pearson, 1905) to simulate passive particle transport through hydrodynamic flow fields on regular grids. Here we provide a brief description of *dorado*; for more information see Hariharan et al. (2020) and the *dorado* documentation. The particle walk algorithm is weighted by local flow direction and water depth, in a manner similar to that of the DeltaRCM model (Liang, Voller, & Paola, 2015; Liang, Geleynse, et al., 2015). For a given grid cell, the downstream direction F^* is computed by a weighted combination of water surface slope (F_{sfc}) and discharge (F_{int}) unit vectors:

$$F^* = \gamma F_{\mathrm{sfc}} + (1-\gamma) F_{\mathrm{int}} \tag{1}$$

where the parameter γ is specified by the user depending on the nature of transport. Particles are then routed based on orientation to the mean flow direction and the depth in each cell, with the routing weight of each cell i given by:

$$w_i = \frac{h_i^{\theta} \max(0, F^* \cdot d_i)}{\Delta_i} \tag{2}$$

where F^* is the local flow direction computed in Equation 1, d_i is the unit vector pointing to downstream cell i, Δ_i is the Euclidian distance to downstream cell i, h_i is the depth of downstream cell i, and the exponent θ is a weighting parameter specified by the user (Liang, Voller, & Paola, 2015; Hariharan et al., 2020). The default value of θ is 1.0, which routes particles proportionally based on flow depth under the assumption that deeper cells receive more flow than their shallower neighbors (in the absence of vertical model resolution). The particle routing in this study uses $\gamma = 0.05$ and $\theta = 1.0$ (Liang, Voller, & Paola, 2015), where routing weights depend mostly on discharge, and therefore the analysis and discussion that follows can be thought of conceptually as water solute transport.

dorado tracks individual paths and travel times of particles as they are routed through a flow field. An effective particle travel distance is computed for each iteration, defined by the Euclidian distance traveled to one of the surrounding eight grid cells projected onto the mean flow vector. The particle travel time $T_{p,i}$ between cell i and cell i+1 is then back-calculated from the effective travel distance and local flow velocities, with a dispersion coefficient applied that allows $T_{p,i}$ to vary stochastically up to 10 percent from the mean velocity.

In a steady flow field, a sufficient number of particles initialized at the domain inflow location and routed through the domain can provide a probabilistic, spatial distribution of particle paths. All hydraulically-connected locations in the flow field have some probability of having a particle pass through. The total travel time for each particle can be computed, and the average travel time for all particles passing through a stationary part of the domain can be computed as well. Particle travel paths are limited, however, to the instantaneous WSE gradient and discharge in the steady flow field, which may only be representing a particular snapshot in time. The flow field may show certain areas of the floodplain as connected hydraulically, but the instantaneous directionality of the water fluxes may cause only certain trajectories to be feasible.

A flow field that changes through time, due to the rising and falling of the flood wave or unsteady precipitation on the floodplain, creates an environment where potential particle paths are highly dependent on when and where particles enter the floodplain from the river. For example, a particle will not move from river to floodplain until the river stage reaches an elevation higher than the elevation of the deepest floodplain channels. Even then, if the floodplain is already inundated from rainfall, the gradient may not allow river water into the floodplain. Only at a higher river stage might the flow direction change. Routing particles through an unsteady flow field is critical to understanding these river-floodplain interactions.

The ANUGA model depth, stage, and momentum outputs were interpolated to a 2-m raster grid, and a new particle "cohort" consisting of 1,000 particles was initialized in the domain every 15 minutes of model simulation time. Two classes of particles were analyzed: river particles and floodplain particles. All river particle cohorts were initialized at the inlet of the domain, while floodplain particles were seeded randomly throughout the floodplain in grid cells with depth greater than 20 cm. Separating particles into these two classes is necessary for distinguishing between patterns of rainfall and river flood processes. Floodplain particles were initialized beginning at simulation hour 45 (the onset of intense rainfall, see Figure 3), while river particles were initialized at simulation hour 60, as flow does not move from river to floodplain until sometime after hour 60. All particle cohorts were routed through the model flow field until simulation hour 120. With 1,000 particles per

15 minutes, the total number of river particles tracked was 240,000, and the total number of floodplain particles was 300,000.

Particle dynamics were quantified in two ways: velocity distributions and residence time distributions. Velocity distributions show the spatial extent of particle paths, as well as the average speed at which particles move through each 2-m grid cell in the model domain. The average time a particle spends in cell (x, y) is calculated as follows:

$$t_{avg,xy} = \sum_{p=1}^{N_p} \frac{0.5 \times (T_{p,i,xy} + T_{p,i+1,xy})}{N_{p,i,xy}} \tag{3}$$

where N_p is the total number of particles, the numerator is the average of travel times for particle p as it entered (iteration i) and as it left (iteration i+1) cell (x, y), and $N_{p,i,xy}$ is the number of times a particle entered cell (x, y). The array is masked for $N_{p,i,xy} = 0$. Then the average flow speed $V_{avg,xy}$ is:

$$V_{avg,xy} = \frac{dx}{t_{avg,xy}} \tag{4}$$

where dx is the cell size. A Gaussian smoothing filter with standard deviation of 0.7 was applied to the $V_{avg,xy}$ array to reduce noise and enhance visualization.

Particle residence time distributions are calculated in the form of the cumulative exit age distribution $F(t)$ (Benjamin & Lawler, 2013):

$$F(t) = \int_0^t \frac{dN_p/dt}{N_{p,tot}} dt \tag{5}$$

where $N_{p,tot}$ is the total number of particles that enter a control volume, dN_p/dt is the rate at which particles exit, and at $t = \infty$, $F(t) = 1$. For this study, we define the control volume as the entire river-right floodplain in the model domain. We track individual particle travel times beginning when they enter (or are seeded in) the floodplain, and ending when they leave:

$$t_p = \sum_{i=1}^{N_i} T_{p,i} \tag{6}$$

where t_p is the total travel time for particle p within the floodplain boundary, N_i is the number of iterations performed while within the boundary, and $T_{p,i}$ is the travel time for each iteration. All values of t_p are sorted in ascending order, and then $F(t_p)$ is simply the cumulative fraction of particles that spent less than t_p in the domain.

4.3 Scaling Analysis to Quantify Lateral Flux

We perform a model scaling analysis, with a goal of quantifying lateral flux between river and floodplain as floodplain channels of various sizes are smoothed out of the model. A set of additional model meshes was developed for this task, each with varying resolution in the subdomain area outlined in Figure 1C. In addition to the 2-m model described in Section 4.1, mesh resolutions of 5 m, 10 m, and 20 m were evaluated, with total element counts of 269,361; 129,051; and 78,752; respectively. Each mesh had the same outer boundary, and the same resolution across the majority of the domain (20 m). All model forcings and other characteristics described above were applied equivalently to each model.

The largest floodplain channel in the model domain is close to 50 m wide, and is located at the western edge of the floodplain on the river right (Figure 1C). However, this channel is not directly connected to the river, and instead drains a wetland (Champion Lake) in the floodplain just upstream of the study area. Within the high-resolution subdomain, the largest floodplain channel is about 10-m wide, which can be seen in the DEM (Figure 1C) along the western edge of the subdomain boundary. In general, channel widths range from this upper limit of 10 m down to the scale of 1-m DEM. The channel leading to the Site 4 location varies in width, and is mostly between 6 and 8-m wide (Figure 1D). The Site 5 location is within a channel that is 4 to 5-m wide. As model resolution is coarsened from 2 m, these channel features become smoothed out (Supporting Information Figure S2).

Lateral flux is computed from each model by drawing several transects parallel to the river at or near the levee crests, at locations where river-floodplain flow connectivity is significant, and computing the time series of flow through each transect. Transect locations were drawn at locations where *dorado* particles entered the floodplain from the river. This calculation shows which channels are sensitive to model resolution, and the extent to which overall flow into the floodplain changes as these channels are smoothed out of the model.

5 Results

5.1 Numerical Model

The numerical model was calibrated to match the observed WSE (relative to NAVD88) at the USGS Moss Bluff gage, and therefore the match between model and observed water level in the main channel is almost exact (Figure 4A). Modeled flow depths in the floodplain were compared with those of the water level loggers at field Sites 4, 5, and 6 (Figure 4B–D). From the beginning of the event (hour 0) to the fluvial peak (hour 96), the range of measured water levels at each site was consistently larger than those from the model. As discussed in Section 3.2, however, vertical positions of the loggers with respect to the floodplain topography are unknown and therefore could not be used as ground-truth depths. For this reason, the measured water levels are most accurately viewed in relative terms.

To evaluate model results in the floodplain against measurements, the measured water level time series was set equal to the model at the end of the 8-day simulation (Figure 4B-D). At this time, water levels at all three sites began to flatten out toward a steady-state condition after river stage dropped below the range of elevations at which river water connects with the floodplain. The model showed similar rates of drainage at each site during this period, and thus simulation day 8 was considered an appropriate point to equate the water level data, as there was less water level change occurring at this time and rainfall and river discharge were no longer actively influencing the sites.

The rate of change of water levels seen in the data during the fluvial peak is captured well in the model at all three sites. The sites are located at various distances from the river, but in each case the model was able to move water to various positions in the floodplain at similar rates shown by the data. At Site 4 (Figure 4B), the timing and rate of drainage during the falling limb is particularly aligned with the data. Of note, however, is that the peak depth from rainfall (between hours 48 and 72) is almost exactly equal to the peak depth during fluvial flooding. The maximum flow depth of about 1.1 m corresponds to the depth of the floodplain channel at this location in the lidar, which shows the channel was reaching bankfull flow in the model at each of these times. It would take a significantly greater flow rate in the river to increase this depth, as the floodplain in this area would have to be fully inundated. Instead, it is clear there is a discrepancy between the 2017 lidar and the 2019 channel topography. The measured depth at the time of installation was 0.9 m, and the logger showed a rise in water level 1.0 m beyond the initial level, implying a total measured channel depth of at least 1.9 m. As such, it is unsurprising that there is a significant vertical offset between modeled and measured water levels at this location.

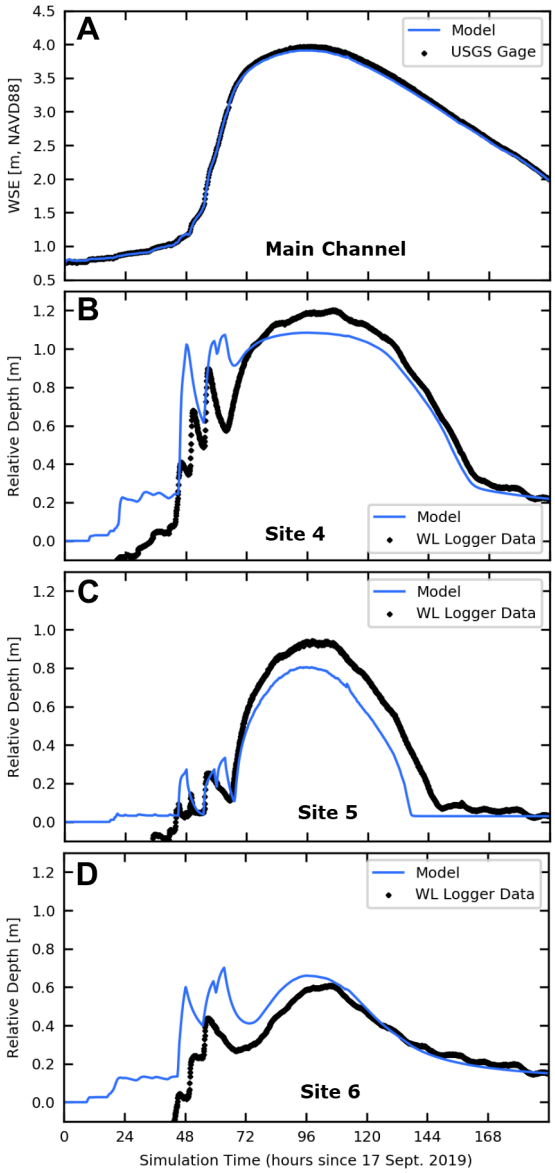

Figure 4. Numerical model water level results (2-m resolution) compared to measured values. (A) WSE plot showing the match between stage measured at the USGS Moss Bluff gage and that of the model. (B) Water level comparison in the Site 4 floodplain channel. (C) Water level comparison in the Site 5 floodplain channel. (D) Water level comparison at Site 6, at the terminus of the floodplain channel containing Site 5.

The rainfall signal at Site 5 was less than at the other two sites (Figure 4C). Located on the levee only 50 m from the river, the area draining to Site 5 is much more limited. Due to its proximity to the river, though, the full signal of the flood wave was observed in the data and the shape of the curve was almost identical to the stage curve at the nearby USGS station. The model also showed a flood wave through this channel with a similar shape to the data, peaking at a depth of 0.8 m. By the time the river flood wave receded, the model at this location dried up completely, while the data showed water remaining in the channel (40 cm, based on depth at install). The Site 5 channel slopes gradually down the levee (at roughly 0.08%), so the presence of a near-constant water depth without additional rain or

river input suggests the logger may have been in a local depression in the channel deeper than indicated by the lidar.

Modeled water depth at Site 6, located just beyond the terminus of the Site 5 channel, also showed a pattern of drainage similar to measured water levels at times beyond the fluvial peak. However, the peak pluvial and fluvial depths in the model were almost identical (0.7 m) but they were different from each other in the data. Like Site 4, water levels increased dramatically from the heavy rainfall, then decreased slightly, before increasing again beyond the maximum level reached during the rainfall period. It is likely that standing water at this location (initial measured water depth here was 57 cm) causes a disagreement between the lidar data and the true bottom of the floodplain basin.

With each of the three successive rainfall bands, the floodplain became increasingly inundated. Maximum inundation extent occurred at simulation hour 63, corresponding to the end of the third rainfall band, where inundation extent was evaluated over the entire river-right floodplain (excluding isolated areas to the river-left) and included all areas with at least 10 cm of depth. At this time, 65 percent of the floodplain was inundated. The floodplain drained between the end of the last rainfall band and the time of river influence. Peak inundation from river flooding occurred at simulation hour 96, when 55 percent of the floodplain was inundated (see Supporting Information animations for modeled changes in inundation extent during the storm). The differences in inundation extent suggest that, for a sub-bankfull flood event lasting only a couple of days, river water may be limited to a smaller portion of the floodplain based on the number and orientation of floodplain channels facilitating this connectivity.

5.2 Particle Routing Analysis

Although the water depths in the floodplain did not exactly match the data, the results of the numerical model showed rates of change and overall hydrodynamic patterns similar to the data. The model can be viewed as a realistic representation of the type of conditions in the Trinity River floodplain during Tropical Storm Imelda, where both pluvial and fluvial flooding were major factors. Using the model flow field for particle routing helps describe and quantify the complex interactions that can occur in low-gradient river floodplains during similar events. By continuously seeding passive particles in the river and floodplain, we can observe the differences between water moved by rainfall and river flooding, and how the dominant forcing can change in the floodplain during a storm. Particle velocity distributions show the spatial distribution of particle paths in two dimensions, along with their average velocities. Residence time distributions (RTDs) inform on flow time scales for particles that move through the floodplain. Both show the distinction and interaction between rainfall and river processes.

Two particle classes were seeded continuously every 15 minutes throughout the storm event: one in the main channel and one distributed randomly throughout the floodplain (see Supporting Information Movies S1 and S2, respectively, for particle animations). Floodplain particles were only seeded in grid cells where water had accumulated to a depth of 20 cm during the prior time step. Particle velocity distributions show the spatial extent of particle paths in two dimensions (Figure 5). During simulation hour 61 while it was still raining heavily, the gradient was from floodplain to river, and river particles remained confined, even though the floodplain was inundated everywhere except the topographic ridges (Figure 5A, seen in lighter shades of gray). At the same time, floodplain particle paths were widely connected (Figure 5D). At simulation hour 72 (panels B and E) it was no longer raining heavily, but the peak river discharge had not arrived yet. Some of the rainwater had drained from the remote areas of the floodplain, and water pooled in the larger floodplain basins slowed down (darker colors) as it left through the outlet to the south. More river particles began to enter the floodplain, mostly from the counter point bar due south of Site 6, but a few began to enter through the floodplain channels near Sites 4 and 5 as well. Finally, at

simulation hour 91 (panels C and F), the river discharge was at its maximum. Floodplain particles (panel F) were limited to the larger floodplain basins, similar to the previous time stamp, but average velocities were slightly higher overall. This is because the river was supplying more water to the floodplain, and thus providing a stronger gradient to the floodplain outlet that was not present at simulation hour 72. As expected for particles originating in the river (panel C), the travel paths were limited to just a fraction of the floodplain, even during peak discharge.

The combined velocity distributions (Figure 5G and H) were computed by taking the average velocity for all particles spending time in a given grid cell. The combined distribution for river particles (Figure 5G) shows that river particle paths always remained within the corridor shown in Figure 5 panels B and C. The velocities also show that river water generally spent less time in the floodplain than rainwater, with the exception of the floodplain in the north corner of the domain, which is very deep and highly-connected to the main channel. The large, dark-colored region of lower floodplain particle velocities (Figure 5H) was inundated throughout the storm, but river particles never reached it. Instead, river particles seemed to bypass this part of the floodplain entirely, while rainwater spent much more time in this area as it drained slowly to the outlet.

For river particles, residence time distributions (RTDs) were combined for cohorts seeded between simulation hours 66 and 90, as there were not enough particles entering the floodplain at earlier times (Figure 6A). For floodplain particles, the combined time window is between simulation hours 46 and 90 (Figure 6B). The limit at simulation hour 90 was chosen because particles were only tracked up to simulation hour 120, and the residence time window observed was limited to 30 hours (Figure 6, x-axis). Ninety-five percent of river particles spent a minimum of five hours in the floodplain (within the model domain), and about 80 percent of particles had residence times less than 10 hours. The five percent of particles with residence times of less than five hours were those that entered the floodplain briefly before returning to the river. The narrower distribution confirmed what can be seen spatially in the velocity distributions (Figure 5G). Floodplain particles had a wider distribution of residence times. Many particles exited the domain quickly if seeded close to the outlet, but 20 percent of floodplain particles remained in the domain for longer than 30 hours, compared to just 10 percent for river particles. Note that the river particle RTDs are composed of less particles by several orders of magnitude, because only a smaller fraction of particles move to the floodplain from the river compared to those that are seeded in the floodplain initially. Also note that the southeastern-most corner of the domain was masked out for the particle analysis because too many river particles were entering the floodplain at this bend and immediately exiting the floodplain due to proximity only, not from faster flow velocities, and this skewed the residence time distributions.

Particle RTDs evolved over the course of the storm (Figure 6B and D). At simulation hour 66, only a small number of river particles entered the floodplain, but that number increased as the storm transitioned to the fluvial phase (Figure 6B). Through this transition, river particles experienced a reduction in minimum residence time as the discharge increased. At higher discharges in the river, more flow moved through the floodplain, increasing velocities and reducing residence times. Floodplain particle RTDs show a wider range of behavior, as there may be more competing factors involved in their movement (Figure 6D). The RTD for the earliest group of particle cohorts, representing most of the 8,000 particles seeded between simulation hours 46 and 48, shows that 90 percent of particles left the floodplain after 15 hours. Fifteen hours corresponds to simulation hour 61, when heavy rainfall was still active. Although the rainfall stopped and started twice during this 15-hour period, the overall period of rainfall flushed the floodplain to some degree, and the result was a nearly uniform distribution. Moving forward in time, the sixth group of cohorts (simulation hours 56-58) marked a transition in the RTD where a greater fraction of particles left the floodplain faster, but the remaining particles spent longer than those from 10 to 12 simulation hours prior. The transition can be attributed to the period between heavy rainfall and peak

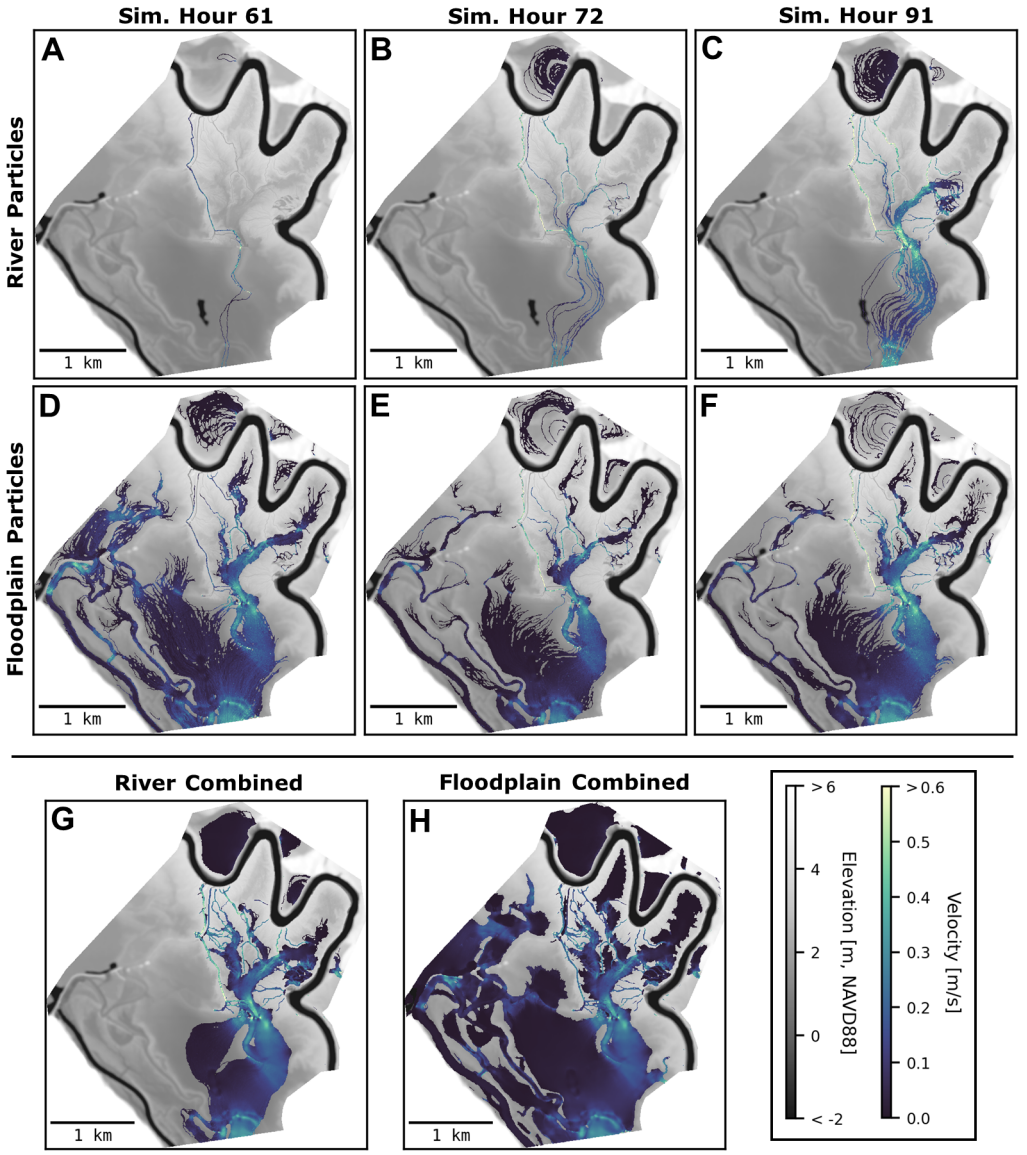

Figure 5. Average particle velocities for river particles (top row) and floodplain particles (second row). (A), (B), and (C) Velocity distributions for river particles at simulation hours 61, 72, and 91, respectively. (D), (E), and (F) Velocity distributions for floodplain particles at simulation hours 61, 72, and 91, respectively. Combined velocity distributions for (G) river and (H) floodplain particles.

discharge. The longer residence times represent particles stranded in remote areas of the floodplain as rainwater drained, and the shorter residence times were a result of floodwaters accumulating closer to the outlet, where newly seeded particles then had less distance to travel to the outlet. Particle cohorts seeded between simulation hours 56 and 62 began to show an increasingly greater fraction with shorter residence times, due to being seeded *after* the longest pause in rainfall (see Figure 3), but also an increasingly greater fraction with longer residence times, due to the heavy rainfall stopping for good after simulation hour 63. After the rainfall phase, the RTD became more consistent through time, as the remote areas of the floodplain drained and inundation became dominated by river water. Average residence times reached a maximum (lowest red curves, Figure 6D) before reducing again during peak discharge when velocities were higher (bright yellow curves).

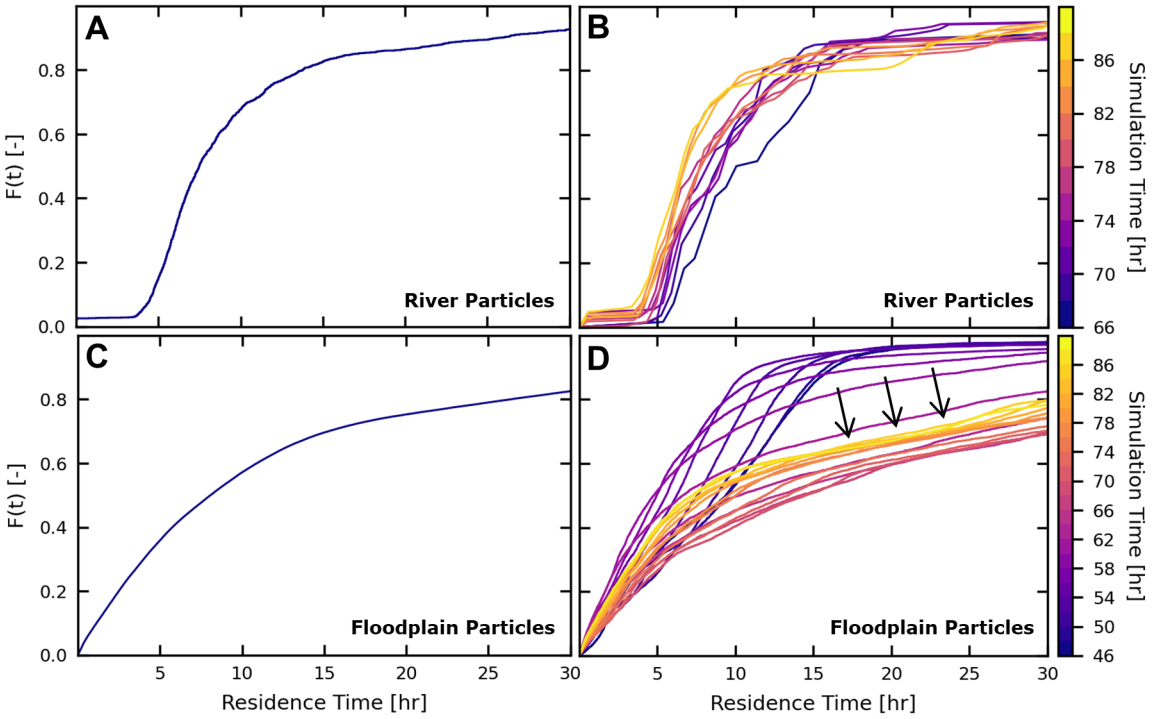

Figure 6. Cumulative Residence Time Distributions (RTDs) for river (top row) and floodplain (bottom row) particles. (A) Combined RTD for particles seeded in the river between simulation hours 66 and 90. (B) RTDs for river particles, grouped in intervals of two simulation hours, where the darkest purple line is the combined RTD of particles seeded between simulation hours 66 and 68, and the lightest yellow line represents particles seeded between simulation hours 88 and 90. (C) Combined RTD for particles seeded in the floodplain between simulation hours 46 and 90. (D) RTDs for floodplain particles. The darkest purple line represents particles seeded between simulation hours 46 and 48, and the lightest yellow line represents particles seeded between simulation hours 88 and 90. The black arrows represent the time after rainfall ended, when river stage was increasing.

At field Site 6, located at the terminus of a floodplain channel in a small floodplain basin, a noteworthy reversal of flow occurred in the model that is described well by particle routing (Supporting Information Movie S3). One hundred particles per 15 minutes were seeded at the Site 6 location. During the early rainfall phase, particles flowed directly to the floodplain outlet with a nearly constant residence time of eight hours (Figure 7A and C, purple curves). After the rainfall stopped, flow paths remained similar, and residence times remained nearly constant at five hours for 80–90 percent of particles. Beginning at about simulation hour 78, as more river flow was conveyed to the floodplain from the local floodplain channel and the bend to the south, the small basin began to fill up, causing new particles to become trapped there (Figure 7B and C, orange curves). This reversal lasted until about simulation hour 84, very close in time to the peak discharge, when the floodplain basin water levels equilibrated with the river, and the flow direction reversed again. Particles then returned to the original flow path, with nearly constant residence times of six hours for 90 percent of particles (Figure 7C, yellow curves). The flow reversal lasted for only six hours, but many particles seeded around this time had residence times exceeding 30 hours (Figure 7C, orange curves). This type of flow reversal represents a drastic change in average residence times, and could have significant implications for floodplain processes when scaled to entire floodplain systems.

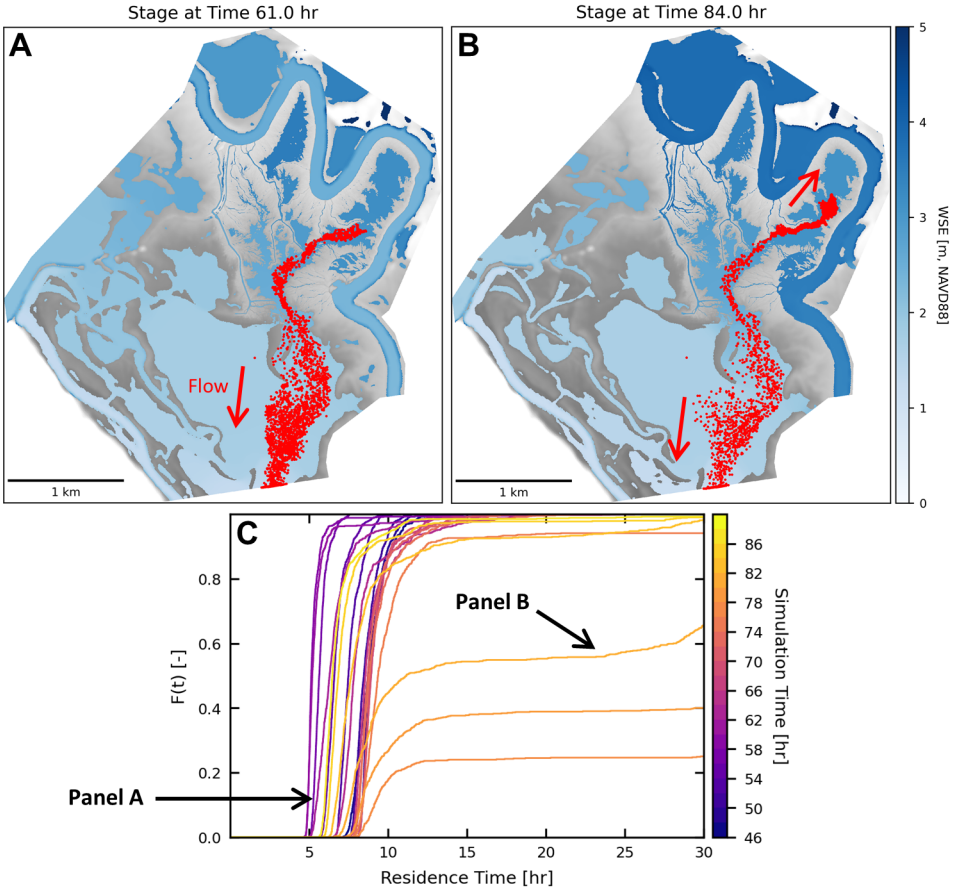

Figure 7. Flow patterns illustrated by particles seeded at Site 6. (A) State of particles at simulation hour 61. Heavy rainfall on the floodplain moved all particles toward the floodplain outlet. (B) State of particles at simulation hour 84. Flow reversal due to fluvial flooding pushed particles farther into the local floodplain basin. The flow reversal lasted from simulation hour 78 to 84, after which particles began flowing back toward the floodplain outlet. (C) RTDs for Site 6 particles grouped every two simulation hours, from simulation hour 46 (darkest purple curve) to 90 (lightest yellow curve). Three orange curves at the bottom right of the plot represent six simulation hours of particles that experienced the flow reversal shown in panel B. The black arrows point to RTDs corresponding to figure panels A and B.

5.3 Role of Floodplain Channels

Changes in numerical model resolution had a varying effect on modeled river-floodplain connectivity. As model resolution was reduced, flow depths through the floodplain channels of Sites 4 and 5 were reduced (Figure 8A and B). These features are completely sub-grid at 20-m model resolution. The flow depth at Site 4 was much greater in the 10-m model than in the 20-m model, although the fluvial signal was dampened compared to the models with further refinement. Because the Site 4 channel is several meters wider than the Site 5 channel, the 10-m model resolved the Site 4 channel to a much greater degree (see Supporting Information Figure S2 for channel cross-section geometry at each model resolution). At Site 4, the difference in peak depth between the two high-resolution models was 12 cm, or 11 percent of the 2-m flow depth, while the difference in peaks at Site 5 was 33 cm, or 41 percent of the 2-m flow depth. This distinction shows that the smaller channel was more dependent

on model resolution, although at both sites, capturing the full range of hydrodynamics was dependent on resolution finer than the width of the channel.

There was very little distinction between models at the Site 6 floodplain basin (Figure 8C). The difference in peak flow depth between the 20-m and 2-m models was only 13 cm, while flow depths in the three higher resolution models were virtually identical. It is not surprising that flow depths in the channelized locations were more sensitive to model resolution than depths in the wider, flatter Site 6 location. However, even though Site 6 was located just beyond the terminus of the Site 5 channel, the increased flow quantity delivered from Site 5 (Figure 8B) had almost no effect on flow depths at Site 6. Instead, the majority of flow supplied to Site 6 must have originated from sources other than smaller, mesh-scale floodplain channels.

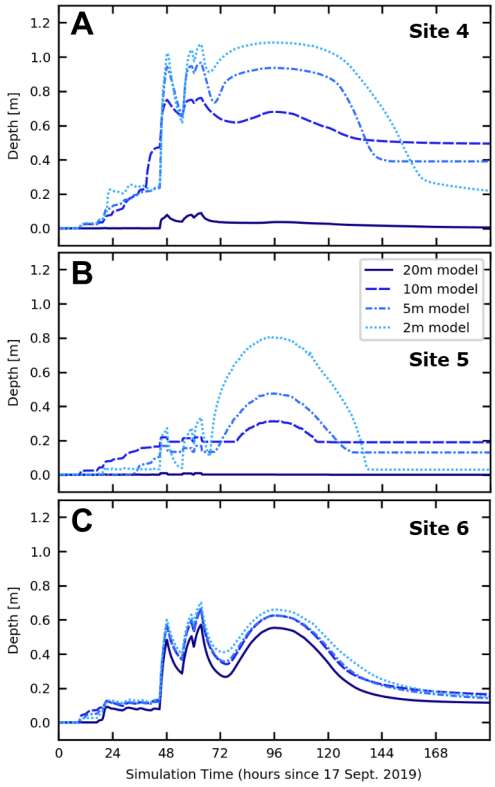

Figure 8. Model flow depths for model resolutions of 20 m, 10 m, 5 m, and 2 m in the floodplain at (A) Site 4, (B) Site 5, and (C) Site 6.

Lateral flux between the river and floodplain changed dramatically at some locations along the levee, and less so at others, with increasing model resolution (Figure 9). Transects in Figure 9 are labeled in increasing order moving downstream, beginning with Transects A and B across the two largest floodplain channels in the domain, Transect C across the channel that leads to field Site 4, transect D across two smaller channels (one of which leads to Sites 5 and 6), Transect E across the wide counter point bar near Site 6 referenced in Section 5.2, and Transect F across a series of smaller levee channels at the same river bend as Transect E. Flow through Transect E is shown as a red dotted line because it is different from the others in that it does not represent a floodplain channel. Flow over this counter point bar into the floodplain was highest in the 20-m model (12 m^3/s, Figure 9B) and lowest in the 2-m model (10 m^3/s, Figure 9E), representing a much smaller difference across models than in many of the other floodplain channels. The opposite was true with

the large channel at Transect A, where the flow through this channel was highest at 2-m resolution (13.5 m^3/s) and lowest at 20-m resolution (8.8 m^3/s). The behavior at Transect B was less straightforward, as the peak flow was larger in the two end-member models than in the mid-resolution models, but still the flow here was greater in all models than any of the downstream channelized transects. At Transect C (leading to Site 4), the flow increased from near zero with 20-m resolution to a maximum of 6.6 m^3/s with 2-m resolution, which corresponds to the differences in depth shown in Figure 8A. Similar flow increases were seen with increasing model resolution at Transects D and F, but the total increase was less, as these are smaller channels. Lastly, negative flow through many of the channels, and across the counter point bar, during the period of heavy rainfall represents flow into the channel from the floodplain. The magnitude of reverse flow increased with increasing model resolution, particularly at Transects A and C. This result shows that some floodplain channels can be important conveyors of bidirectional flow between river and floodplain.

Despite some of the differences shown in Figure 9, particle dynamics in the overall floodplain were largely unaffected by model resolution. Floodplain residence times were very similar for model resolutions of 2 m, 5 m, and even 10 m (Figure 10A and B). For both particle classes, some differences were observed with the coarser, 10-m resolution, but for the most part the residence time distributions look as they do in Figure 6. This result is supported by the model flow depths at Site 6, where little difference was observed between models of varying resolution (Figure 8C). Although the locations with the highest flow rates entering the floodplain did experience flow changes at different resolutions (Figure 9), the difference in volumes was not as significant as suggested by the model results at Sites 4 and 5 (Figure 8A and B). The similarity in floodplain RTDs at different resolutions may be due to the consistent influence of the largest sources of flux (Transects A, B, and E) across all model resolutions, implying that the smaller floodplain channels (e.g., Sites 4 and 5, Transects C and D) are less important contributors of flow to the floodplain.

Particles released within the Site 4 floodplain channel reinforced the idea that there can be a significant effect of resolution locally (Figure 10C). RTDs for the 2-m and 5-m resolution models were almost identical, but the 10-m model's failure to resolve the Site 4 channel well completely changed the conveyance through the channel. Despite the fact that the majority of the floodplain beyond this local channel had a similar flow field in the model at all mesh resolutions, the lack of resolution here served as a local bottleneck for river water that would have otherwise moved to the floodplain through this particular channel. However, some fraction of particles still moved through the floodplain channel, even at 10-m resolution. Particle animations (Supporting Information Movie S4) show that flow was only conveyed through this channel when rainfall was active, and directly following the peak discharge. During the pauses in rainfall, the flow drained from the channel and particles became stuck, to be flushed out when the rainfall resumed. Particles remained stuck in the channel for the period between heavy rainfall and peak discharge (simulation hours 63-92), after which particles were conveyed through the floodplain due to sufficient river flow. Flow was cut off once again at simulation hour 112. This result aligns with the range of depths at this location in the 10-m model (Figure 8A), and the range of flows (Transect C, Figure 9), where the window of changing depths in the channel was much more limited. In general, the RTDs for Site 4 particles and the model depth curves (Figure 8A and B) show the importance of model resolution on local processes where features near the scale of the mesh resolution are relevant.

The impact of model resolution could be seen in the channels close to Site 4 as well. Field observations at Site 4 did not show any flow reversals as the event transitioned from rainfall to river-dominated (Figure 2B), and thus all particles released at Site 4 flowed south into the floodplain (locally, although Figure 9E shows that a flow reversal occurred in the model closer to the river). But particle animations (Supporting Information Movie S5) show that for particles released at Site 4 during the rainfall phase, a portion of flow was siphoned into the larger floodplain channel just west of Site 4 (corresponding to Transect A

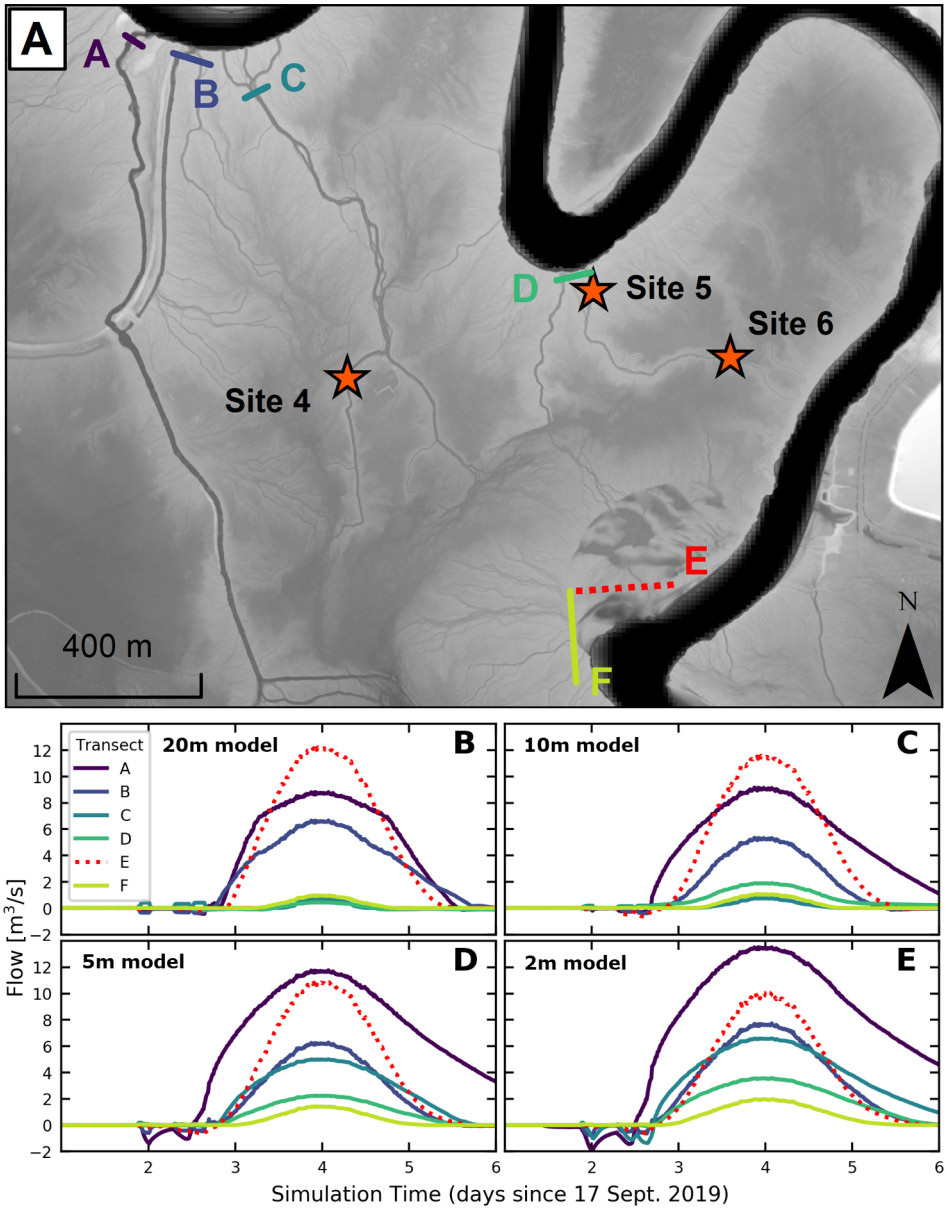

Figure 9. Modeled lateral flux between river and floodplain. (A) Site map of transect locations where lateral flux is computed. Transect E represents a non-channelized source of exchange. Flow through transects in (B) 20-m model, (C) 10-m model, (D) 5-m model, and (E) 2-m model.

in Figure 9), where local rainfall was moving water into the river. At the time when rainfall stopped, the flow reversed, and the gradual rise in river water levels did not allow particles to move into the river through these channels any longer. Particles only moved in this way with model resolution of 5 m or finer. The 10-m model could not resolve a deep enough floodplain channel to convey particles.

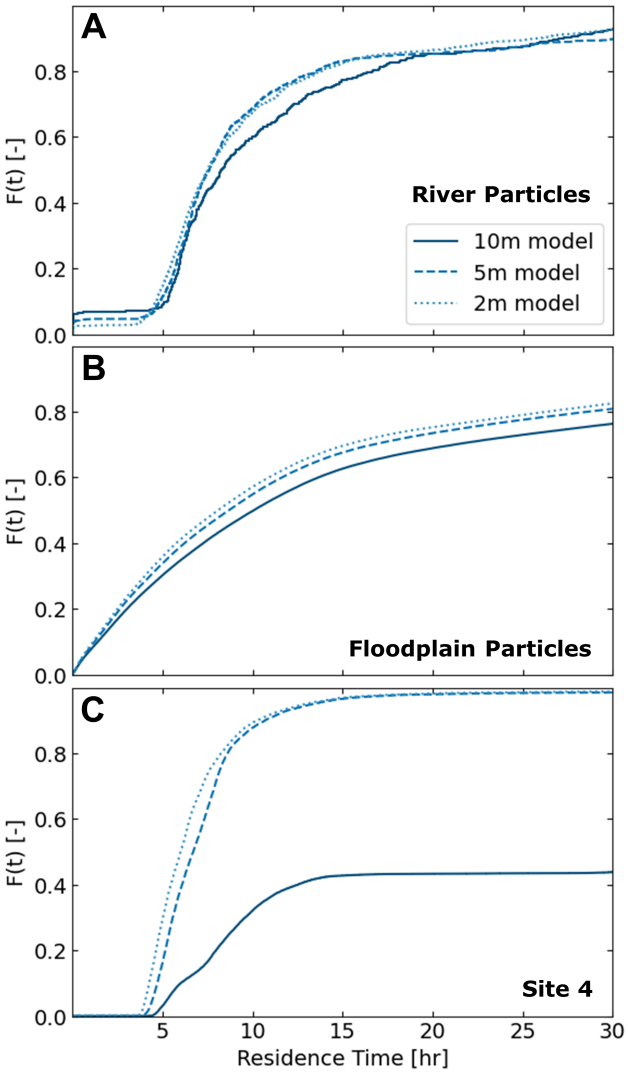

Figure 10. RTDs with different model resolutions, for (A) river particles released between simulation hours 66 and 90, (B) floodplain particles released between simulation hours 46 and 90, and (C) particles released in the Site 4 floodplain channel between simulation hours 46 and 90.

6 Discussion

6.1 Pluvial and Fluvial Flooding Interactions

Field data collected in the Trinity River floodplain during Tropical Storm Imelda showed distinct signals of flooding from the river and from rainfall. The relative timing of rainfall and the peak discharge at the study site created an interesting transition of floodplain hydrodynamics from being pluvial-driven to fluvial-driven. The data showed that with heavy rainfall on the floodplain, river-floodplain connectivity can occur many hours (in this case about 24 hours) prior to the flood wave, and that this connectivity is influenced by floodplain channel topography. Furthermore, the extent of connectivity may be reduced or removed completely if rainfall intensity lessens or stops altogether for a period of time before peak river discharge. The data make clear that pluvial flooding can be an important component of river-floodplain connectivity.

Numerical modeling and particle routing analysis reinforced many of the patterns seen in the data relating the timing mismatch of pluvial and fluvial flooding to bidirectional connectivity between the river and floodplain. Studies have shown that river-floodplain connectivity can be established at river stages less than bankfull (Mertes, 1997; Nicholas & Mitchell, 2003; Trigg et al., 2012; Czuba et al., 2019), but the current study showed that connectivity can be established from pluvial flooding at river stages even less than the elevation of the deepest floodplain channels. In fact, model data and measurements from Site 1 show that heavy rainfall on a saturated floodplain can provide a competing force against river waters that would otherwise enter the floodplain. And while flow directed toward the river may only occur during a certain phase of a storm, even when a flow reversal occurs river flux into the floodplain may be limited by a reduced gradient from the presence of rainwater.

However, many areas of the floodplain can be activated by pluvial flooding that may not otherwise be reached by river water. The large rain bands observed during the storm and applied to the model inundated a majority of the floodplain (Supporting Information Movie S2). In many locations, the rainwater drained rapidly (even between successive bands), while in other locations it collected and slowed down. If given enough time at peak discharge, river water may be able to reach more remote areas of the floodplain. But for events like Imelda where the discharge is sub-bankfull and the flood wave lasts for only a couple of days, river flooding is limited in time and space. In this case, the presence of substantial pluvial flooding on the floodplain reduces the available floodplain storage and increases depths, potentially preventing river water from reaching those areas of the floodplain that are not as directly supplied by flow from floodplain channels.

The results discussed here can and should be considered in other river systems with similar characteristics. In lowland systems with the potential for intense precipitation, such as other rivers near the Gulf Coast, pluvial flooding can be a major factor. It is likely, then, that similar patterns of competition between pluvial and fluvial flooding can occur during sub-bankfull discharge. In a different location, even somewhere else along the Trinity River, the results of this study (floodplain residence times and velocities) would likely change to some extent due to topographic differences. However, we anticipate that similar patterns would emerge. The takeaways below of nutrient removal and sediment transport can apply to any system where similar flooding conditions are possible.

6.2 Implications for Nutrient Removal and Sediment Transport

Understanding the mechanisms controlling river-floodplain connectivity is important for understanding how many floodplain processes work. Floodplains, especially those near the coast, are known to act as sinks for nutrients present in river water, such as carbon and nitrogen (Tockner et al., 1999; Aufdenkampe et al., 2011; Noe et al., 2013; Wolf et al., 2013; Cheng & Basu, 2017), and for sediment (Tockner et al., 1999; Verhoeven et al., 2001; Schulz et al., 2003; Day et al., 2008; Juez et al., 2019). In some circumstances, floodplains can be a source of dissolved nutrients (Tockner et al., 1999). We have shown that pluvial flooding has a significant role in river-floodplain connectivity, and the implications for floodplain processes related to sediment retention and nutrient removal are numerous.

River-floodplain connectivity is typically studied as a process that is initiated from the river. From this viewpoint, river water spreads into the floodplain over a range of sufficiently high discharges, bringing sediment and solutes to the floodplain. This modeling study showed that there can be a competing gradient between fluvial and pluvial floodwaters, which may reduce the river water that moves into the floodplain, and thus reduce the transport of constituents to the floodplain where they are processed. When the river stage becomes high enough for flow to move into the floodplain, the presence of rainwater still impacts the dynamics. Spatial distributions of velocity (Figure 5) from particle routing analysis show that, for the domain studied, the reach of river water is limited to only a

fraction of the floodplain. If there had been no rainwater in the floodplain, the river water and its constituents would have room to spread to a much larger area. Because the path of river particles is restricted to a relatively narrow corridor of the floodplain, residence times for river particles may be less than they otherwise would be. During peak discharge, RTDs showed that 80 percent of river particles move through the floodplain in about five to seven hours (Figure 6C). In contrast, particles randomly sampled in the floodplain during peak discharge show a much wider range of residence times depending on when and where they are seeded (Figure 6D). If we removed from consideration the fraction of sampled floodplain particles seeded close to the outlet, the distribution would be even wider. This result indicates that the active (high-velocity) portion of the floodplain is within the corridor of river particle paths shown in the velocity distributions (Figure 5G), and the water in the remainder of the floodplain that mostly originated as rainwater is slower moving and less active (Figure 5H). So although inundation maps would show water throughout the floodplain, these results show that it is possible for river water and its dissolved nutrients to short-circuit a large portion of the floodplain, potentially bypassing crucial floodplain ecosystem processes.

The routing parameters used in the particle analysis assume that each particle moves as a passive tracer. Particles, therefore, more closely represent solutes rather than sediment. However, sediment dynamics may be inferred from flow patterns, average velocities, and residence times in the floodplain. Similar to dissolved nutrients, sediment flux from river to floodplain is dependent on the flow gradient, and it is less likely that floodplain sedimentation will occur if the dominant flow direction is toward the river. Again, floodplains already inundated with rainwater may reach equilibrium with the river more quickly, and reduce the window of time where sediment can be transported out of the river. For sediment that does enter the floodplain, sediment deposition is dependent on flow velocities and residence times, which in turn are dependent on the flow interactions that occur during the storm event. Residence times are shortest during peak rainfall and peak discharge when velocities are higher, but in between they can be significantly longer. So pluvial flooding can reduce overall river flow to the floodplain, but the increase in total floodplain volume due to rainwater may increase residence times. The dynamic nature of pluvial and fluvial compound flooding creates conditions for sediment transport and deposition that can change dramatically over the course of an event. In environments where pluvial flooding can be substantial, sediment dynamics should be considered and modeled within this context.

6.3 Role of Floodplain Channels and Model Resolution

In floodplain systems where connectivity is truly limited to smaller floodplain channels (during sub-bankfull flow conditions), mesh resolution could be critical for modeling lateral exchange. The model domain used in this study was chosen partly because there were several floodplain channels of various scales present that had been shown by field observations to convey significant flow. Model results showed that for processes in the overall floodplain, resolving those channels was not always important. A large fraction of flow from the river was supplied by a river bend that was connected to the floodplain at low WSE and over a longer length than individual floodplain channels. This river bend consists of a low-lying counter point bar, where the bank-line location is not bounded by a levee (Transect E, Figure 9). Meanwhile, the Site 6 location was located at the end of the Site 5 channel, but as the Site 5 channel was smoothed out by decreasing model resolution, water depths at Site 6 showed little sensitivity to resolution changes. Alternatively, flow over the nearby counter point bar changed much less with model resolution, and we can say that connectivity between the river and this portion of the floodplain near Site 6 is less dependent on nearby floodplain channels.

The lateral flux analysis showed that the largest floodplain channels conveyed flow to the floodplain at rates similar to the wide counter point bar, and these flows were much less sensitive to changes in model resolution than the smaller channels of Sites 4 and 5.

River particle RTDs, meanwhile, did not change with model resolution. When we combine these observations, it is apparent that flow to the floodplain and flow patterns within the floodplain are controlled by a combination of the largest floodplain channels and wider depressions in the levee. For the smaller channels such as Site 4, model results showed that changes in flow magnitude and direction occur in these channels only when they are resolved sufficiently (Figure 9 and 10). Model resolution can then be important for understanding local processes, and could even be necessary for processes in the larger floodplain for systems where lateral exchange is completely limited to smaller topographic features.

For numerical modeling applications in other river-floodplain systems, or even other locations on the Trinity River, running low-cost model simulations prior to detailed investigation can provide guidance on the major sources of lateral exchange. In some systems it may be the case that the majority of floodplain connectivity is supplied from a small set of large levee depressions such as the counter point bar described above. While in most systems exchange is also likely to occur via smaller floodplain channels, it may not be on a large enough scale to affect overall flow patterns in the larger floodplain. For systems where it is known that floodplain channels are the main drivers of connectivity, it is necessary to resolve them with mesh resolution finer than the scale of those channels. In either case, understanding which features are important in a system can allow modelers to shift computational resources to the most important aspects of their model.

6.4 Importance of Unsteady Modeling

This study described many ways in which floodplain flow patterns can change during a storm. Floodplains can experience periods of rapid pluvial accumulation, draining, flow reversal, and flow deceleration within the span of several days. The complexity of flow through the Trinity River floodplain during combined pluvial-fluvial events shows that it is critical to model these processes in an unsteady way. For applications where the spatial extent of inundation is of interest for various discharges (e.g., Benke et al., 2000; Czuba et al., 2019), steady modeling of river-floodplain connectivity is appropriate. But for problems related to sediment and solute transport into and out of the floodplain, it is crucial to understand how the spatial extent of inundation, flow time scales, and flow directions change over the course of a storm event.

6.5 Limitations and Future Work

The residence times computed in this study were useful for determining how travel times change with different hydrodynamic conditions. But the residence times are relative to the size of the model domain, and cannot be used to assess specific contact times needed for nutrient removal from the water column, for example. It is unclear what happens in the downstream floodplain, and how long water might stay there. It is likely that, for the same flow conditions, residence times change significantly moving down-valley through the lower Trinity River floodplains. It may be worthwhile to increase the model domain to a much larger river-floodplain reach. The domain used in this study needed to be small enough to meet computational constraints for the 2-m simulations, but model results showed that large-scale floodplain processes may not depend on high mesh resolution at the scale of smaller floodplain channels. A less costly numerical mesh that identifies critical topographic features beforehand may be sufficient to perform a similar study on a larger scale. At larger scales, there could be a potential compounding effect of floodplain channels that cannot be seen at the scale of the current model domain. We may also see floodplain flow rejoin the river at points downstream. At these scales, conclusions related to absolute residence times can be sought.

In addition to being limited in space, the particle analysis was also limited in time to just after the passing of the flood wave. The phase of the storm and associated floodplain dynamics related to the falling hydrograph limb and drainage from the floodplain was not

analyzed here. We saw that particles in the floodplain slowed down after the period of intense rainfall ended (Figure 5D and E) and the floodplain began to drain. We also saw that residence times decreased during peak discharge as the total flow in the floodplain increased. It is expected that, following peak discharge, floodplain flow would slow down again as the forcing from the river decreases. This is an additional hydrodynamic phase not captured by the particle analysis, but one that could have implications for sediment deposition and nutrient retention.

The lidar data used for numerical modeling was collected in early 2017, and it is likely that the floodplain topography changed to some degree between then and field data collection (fall 2019). In fact, an even stronger storm (Hurricane Harvey) passed through the region after lidar was collected. Floodplain topography can change over periods of several years, and significant topographic changes have been observed specifically in the Trinity River lidar data between 2011 and 2015 and also between 2015 and 2017 (Hassenruck-Gudipati, 2021). Combined with the possibility of lidar error in the floodplain channels, our model results should be evaluated with this source of error in mind. Still, the model was able to produce flow patterns that generally aligned with the patterns in the field data, and is therefore a useful tool for analyzing hydrodynamics in parts of the floodplain where no data was collected. Even if not an exact replicate of conditions during Tropical Storm Imelda, the relative timing and magnitude of pluvial and fluvial flooding applied to the model created unique conditions related to the competing flooding modes that confirm at a larger spatial extent the observations made from the field data.

Lastly, the model results carry some uncertainty related to the calibrated discharge and rainfall inputs and the downstream boundary condition on the floodplain, both of which should be considered when evaluating the results of this study. It is unclear whether the quasi-transmissive boundary condition at the floodplain outlet fully represents the backwater during Imelda, and thus whether the rate of floodplain drainage in the model was accurate. This uncertainty is related to the discussion of larger model domains, where an expanded domain that includes the floodplain farther downstream might reduce the sensitivity of the model and particle analysis to the applied boundary condition. Various boundary conditions were tested during the calibration phase, but this part of the floodplain was too low in elevation to have an impact on WSEs at any of the field sites for confirmation.

7 Conclusions

This study used field observations, numerical modeling, and Lagrangian particle routing to examine river-floodplain connectivity along the Trinity River during Tropical Storm Imelda. Field data and modeling showed the complex hydrodynamic interactions that can result from heavy pluvial flooding occurring in conjunction with high, sub-bankfull river flow. Floodplain residence times and flow directions in the floodplain can be strongly dependent on the dominant mode of flooding, and can change rapidly during a storm. Residence times were shorter during the periods of active rainfall and peak discharge, and flow slowed considerably in between these phases as flooding transitioned from pluvial to fluvial. Particle routing analysis showed that as river flow moved into a floodplain already inundated from rainwater, the spatial extent of river water was limited to a narrower reach of the floodplain. Without pluvial flooding, river water would likely spread farther into the floodplain where storage is available. Some floodplain channels were shown to facilitate two-way connectivity driven by the timing mismatch between pluvial and fluvial flooding. Although the 5 to 10-m floodplain channels in the study area were shown to be conveyors of lateral exchange, overall processes in the floodplain were unaffected by their resolution in the numerical model, as the majority of lateral exchange came from only a few locations. Variability in how the bank line is constructed also plays an important role in river-floodplain connectivity.

The dynamic environment of competing pluvial and fluvial flooding during a storm has many implications for sediment and nutrient exchange between rivers and floodplains. The

extent to which residence times and flow directions change indicates that optimal conditions for sediment deposition and nutrient retention are limited to only certain phases of a flood event. Enough pluvial flooding occurring prior to peak discharge may prevent river water from entering the floodplain altogether, effectively reducing sediment and nutrient fluxes to the floodplain. Pluvial flooding can also decrease velocities and increase residence times overall, as deep flow can be achieved sooner with less floodplain storage available for the peak river discharge. This study challenges the prevailing perspective that river-floodplain connectivity is dependent only on river discharge, and emphasizes the importance of rainfall as a driver of that connectivity.

Acknowledgments

This work was supported in part by fellowships from the Cockrell School of Engineering and the Graduate School at the University of Texas at Austin, and by the National Science Foundation (EAR-1350336). All modeling was performed using resources provided by the Extreme Science and Engineering Discovery Environment (XSEDE), which is supported by National Science Foundation grant number ACI-1548562. The authors also acknowledge the Texas Advanced Computing Center (TACC) at The University of Texas at Austin for providing HPC resources that have contributed to the research results reported within this paper (`http://www.tacc.utexas.edu`). Partial support for field data collection was provided by the Jackson School of Geosciences at the University of Texas at Austin. Lidar data were obtained from TNRIS, bathymetry data from the Trinity River Authority, and hydrological forcing data were obtained from USGS. The ANUGA and *dorado* model codes are open-source and available online. Field data and model forcing time series can be accessed through the Zenodo repository associated with this manuscript (`https://doi.org/10.5281/zenodo.5628945`). If this manuscript is accepted, all relevant codes will be made available through the Zenodo repository (linked above) by the time of publication. The authors would like to acknowledge Andrew Moodie, Eric Prokocki, and Tian Dong for their feedback on this research. The authors report no conflicts of interest.

References

Alsdorf, D., Bates, P., Melack, J., Wilson, M., & Dunne, T. (2007). Spatial and temporal complexity of the Amazon flood measured from space. *Geophysical research letters*, *34*(8). doi: 10.1029/2007GL029447

Asselman, N. E. M., & Middelkoop, H. (1995). Floodplain sedimentation: Quantities, patterns and processes. *Earth Surface Processes and Landforms*, *20*(6), 481–499. doi: 10.1002/esp.3290200602

Aufdenkampe, A. K., Mayorga, E., Raymond, P. A., Melack, J. M., Doney, S. C., Alin, S. R., ... Yoo, K. (2011). Riverine coupling of biogeochemical cycles between land, oceans, and atmosphere. *Frontiers in Ecology and the Environment*, *9*(1), 53–60. doi: https://doi.org/10.1890/100014

Benjamin, M. M., & Lawler, D. F. (2013). *Water quality engineering: Physical/chemical treatment processes*. Hoboken, NJ: John Wiley & Sons, Inc.

Benke, A. C., Chaubey, I., Ward, G. M., & Dunn, E. L. (2000). Flood pulse dynamics of an unregulated river floodplain in the southeastern U.S. coastal plain. *Ecology*, *81*(10), 2730–2741.

Byrne, C. F., Stone, M. C., & Morrison, R. R. (2019). Scalable flux metrics at the channel-floodplain interface as indicators of lateral surface connectivity during flood events. *Water Resources Research*, *55*(11), 9788–9807.

Chen, X. C. L., Stone, M. C., & Acharya, K. (2020). Assessing connectivity between the river channel and floodplains during high flows using hydrodynamic modeling and particle tracking analysis. *Journal of Hydrology*, *583*, 124609. doi: 10.1016/j.jhydrol.2020.124609

Cheng, F. Y., & Basu, N. B. (2017). Biogeochemical hotspots: Role of small water bodies

in landscape nutrient processing. *Water Resources Research*, *53*(6), 5038–5056. doi: 10.1002/2016WR020102

Chow, V. T. (1959). *Open-channel hydraulics*.

Covino, T. (2017). Hydrologic connectivity as a framework for understanding biogeochemical flux through watersheds and along fluvial networks. *Geomorphology*, *277*, 133–144. doi: 10.1016/j.geomorph.2016.09.030

Czuba, J. A., David, S., Edmonds, D. A., & Ward, A. S. (2019). Dynamics of surface-water connectivity in a low-gradient meandering river floodplain. *Water Resources Research*, *55*(3), 1849–1870. doi: 10.1029/2018WR023527

David, S. R., Edmonds, D. A., & Letsinger, S. L. (2017). Controls on the occurrence and prevalence of floodplain channels in meandering rivers. *Earth Surface Processes and Landforms*, *42*, 460–472. doi: 10.1002/esp.4002

Davies, G., & Roberts, S. (2015). Open source flood simulation with a 2D discontinuous-elevation hydrodynamic model. In *Proceedings of MODSIM 2015*.

Day, G., Dietrich, W. E., Rowland, J. C., & Marshall, A. (2008). The depositional web on the floodplain of the Fly River, Papua New Guinea. *Journal of Geophysical Research: Earth Surface*, *113*, F01S02. doi: 10.1029/2006JF000622

Gurnell, A. M., Corenblit, D., de Jalón, D. G., del Tánago, M. G., Grabowski, R. C., O'Hare, M. T., & Szewczyk, M. (2016). A conceptual model of vegetation–hydrogeomorphology interactions within river corridors. *River Research and Applications*, *32*(2), 142–163. doi: 10.1002/rra.2928

Hariharan, J., Wright, K., & Passalacqua, P. (2020). *dorado*: A Python package for simulating passive Lagrangian particle transport in shallow-water flows. *Journal of Open Source Software*, *5*(54), 2585. doi: 10.21105/joss.02585

Harvey, J., & Gooseff, M. (2015). River corridor science: Hydrologic exchange and ecological consequences from bedforms to basins. *Water Resources Research*, *51*, 6893-–6922. doi: 10.1002/2015WR017617

Hassenruck-Gudipati, H. J. (2021). *Understanding fluvial topography: Morphodynamic processes that build river levees and cut terraces* (Unpublished doctoral dissertation). The University of Texas at Austin, Austin, TX, USA. (115 pp.)

Hughes, F. M. R., Adams, W. M., Muller, E., Nilsson, C., Richards, K. S., & et al., N. B. (2001). The importance of different scale processes for the restoration of floodplain woodlands. *Regulated Rivers: Research & Management: An International Journal Devoted to River Research and Management*, *17*, 325–345. doi: 10.1002/rrr.656

Juez, C., Schärer, C., Jenny, H., Schleiss, A. J., & Franca, M. J. (2019). Rapid mapping of ultrafine fault zone topography with structure from motion. *Water Resources Research*, *55*(11), 9072–9091. doi: 10.1029/2019WR024989

Junk, W. J., Bayley, P. B., & Sparks, R. E. (1989). The flood pulse concept in river-floodplain systems. In G. P. Dodge (Ed.), *Proceedings of the International Large River Symposium. Canadian Special Publication in Fisheries and Aquatic Science* (Vol. 106, pp. 110–127).

Kondolf, G. M., Boulton, A. J., O'Daniel, S., Poole, G. C., Rachel, F. J., Stanley, E. H., ... Nakamura, K. (2006). Process-based ecological river restoration: Visualizing three-dimensional connectivity and dynamic vectors to recover lost linkages. *Ecology and Society*, *11*(2).

Kufel, L., & Leśniczuk, S. (2014). Hydrological connectivity as most probable key driver of chlorophyll and nutrients in oxbow lakes of the bug river (Poland). *Limnologica*, *46*, 94–98. doi: 10.1016/j.limno.2013.10.008

Kupfer, J. A., Meitzenand, K. M., & Gao, P. (2015). Flooding and surface connectivity of Taxodium-Nyssa stands in a southern floodplain forest ecosystem. *River Research and Applications*, *31*(10), 1299–1310. doi: 10.1002/rra.2828

Latto, A., & Berg, R. (2020). *Tropical Cyclone Report, Tropical Storm Imelda (AL112019) 17–19 September 2019* (Tech. Rep.). National Hurricane Center.

Lesack, L. F. W., & Melack, J. M. (1995). Flooding hydrology and mixture dynamics of lake water derived from multiple sources in an Amazon floodplain lake. *Water Resources*

Research, *31*(2), 329–345. doi: 10.1029/94WR02271

Lewin, J., & Ashworth, P. A. (2014). The negative relief of large river floodplains. *Earth Science Reviews*, *129*, 1–23. doi: 10.1016/j.earscirev.2013.10.014

Liang, M., Geleynse, N., Edmonds, D. A., & Passalacqua, P. (2015). A reduced-complexity model for river delta formation - Part II: Assessment of the flow routing scheme. *Earth Surface Dynamics*, *3*, 87–104. doi: 10.5194/esurf-3-87-2015

Liang, M., Voller, V. R., & Paola, C. (2015). A reduced-complexity model for river delta formation - Part I: Modeling deltas with channel dynamics. *Earth Surface Dynamics*, *3*, 67–86. doi: 10.5194/esurf-3-67-2015

Lowell, N. S., Walsh, D. R., & Pohlman, J. W. (2015). A comparison of tilt current meters and an acoustic doppler current meter in vineyard sound, Massachusetts. In *2015 IEEE/OES Eleventh Current, Waves and Turbulence Measurement (CWTM)* (pp. 1–7). doi: 10.1109/CWTM.2015.7098135

Mann, C. J., & Wetzel, R. G. (1995). Dissolved organic carbon and its utilization in a riverine wetland ecosystem. *Biogeochemistry*, *31*(2), 99–120.

Marriott, S. (1992). Textural analysis and modelling of a flood deposit: River Severn, UK. *Earth Surface Processes and Landforms*, *17*(7), 687–697. doi: 10.1002/esp.3290170705

Mason, J., & Mohrig, D. (2018). Using time-lapse lidar to quantify river bend evolution on the meandering coastal Trinity River, Texas, USA. *Journal of Geophysical Research: Earth Surface*, *123*(5), 1133–1144. doi: 10.1029/2017JF004492

Melack, J. M., & Forsberg, B. (2001). Biogeochemistry of Amazon floodplain lakes and associated wetlands. In M. E. McClain, R. L. Victoria, & J. E. Richey (Eds.), *Biogeochemistry of the Amazon Basin and its Role in a Changing World* (pp. 235–276). New York: Oxford Univ. Press.

Mertes, L. A. K. (1997). Documentation and significance of the perirheic zone on inundated floodplains. *Water Resources Research*, *33*(7), 1749–1762.

Mertes, L. A. K., Daniel, D. L., Melack, J. M., Nelson, B., Martinelli, L. A., & Forsberg, B. R. (1995). Spatial patterns of hydrology, geomorphology, and vegetation on the floodplain of the Amazon River in Brazil from a remote sensing perspective. *Geomorphology*, *13*(1-4), 215–232.

Mungkasi, S., & Roberts, S. G. (2011). A finite volume method for shallow water flows on triangular computational grids. In *Proc. 2011 Int. Conf. Advanced Computer Science and Information System (ICACSIS)* (pp. 79–84).

Mungkasi, S., & Roberts, S. G. (2013). Validation of ANUGA hydraulic model using exact solutions to shallow water wave problems. *Journal of Physics: Conference Series*, *423*(1).

Nicholas, A. P., & Mitchell, C. A. (2003). Numerical simulation of overbank processes in topographically complex floodplain environments. *Hydrological Processes*, *17*, 727–746. doi: 10.1002/hyp.1162

Nielsen, O., Roberts, S., Gray, D., McPherson, A., & Hitchman, A. (2005). Hydrodynamic modelling of coastal inundation. In *Proceedings of MODSIM 2005.*

Noe, G. B., & Hupp, C. R. (2005). Carbon, nitrogen, and phosphorus accumulation in floodplains of Atlantic Coastal Plain rivers, USA. *Ecological Applications*, *15*(4), 1178–1190. doi: 10.1890/04-1677

Noe, G. B., Hupp, C. R., & Rybicki, N. B. (2013). Hydrogeomorphology influences soil nitrogen and phosphorus mineralization in floodplain wetlands. *Ecosystems*, *16*(1), 75–94. doi: 10.1007/s10021-012-9597-0

Park, E., & Latrubesse, E. M. (2017). The hydro-geomorphologic complexity of the lower Amazon River floodplain and hydrological connectivity assessed by remote sensing and field control. *Remote Sensing of Environment*, *198*, 321–332. doi: 10.1016/j.rse.2017.06.021

Pearson, K. (1905). The problem of the random walk. *Nature*, *72*(1867), 342–342.

Phillips, J. D., & Slattery, M. C. (2007). Downstream trends in discharge, slope, and stream power in a lower coastal plain river. *Journal of Hydrology*, *334*, 290–303. doi:

10.1016/j.jhydrol.2006.10.018

Phillips, J. D., Slattery, M. C., & Musselman, Z. A. (2004). Dam-to-delta sediment inputs and storage, lower Trinity River, Texas. *Geomorphology*, *62*(1–2), 17–34. doi: 10.1016/j.geomorph.2004.02.004

Roberts, S., Nielsen, O., Gray, D., Sexton, J., & Davies, G. (2015). ANUGA User Manual [Computer software manual].

Roley, S. S., Tank, J. L., & Williams, M. A. (2012). Hydrologic connectivity increases denitrification in the hyporheic zone and restored floodplains of an agricultural stream. *Journal of Geophysical Research: Biogeosciences*, *117*(G3).

Rowland, J. C., Dietrich, W. E., Day, G., & Parker, G. (2009). Formation and maintenance of single-thread tie channels entering floodplain lakes: Observations from three diverse river systems. *Journal of Geophysical Research: Earth Surface*, *114*(F02013). doi: 10.1029/2008JF001073

Schulz, M., Kozerski, H., Pluntke, T., & Rinke, K. (2003). The influence of macrophytes on sedimentation and nutrient retention in the lower River Spree (Germany). *Water Research*, *37*, 569–578. doi: 10.1016/S0043-1354(02)00276-2

Smith, V. B., Mason, J., & Mohrig, D. (2020). Reach-scale changes in channel geometry and dynamics due to the coastal backwater effect: the lower Trinity River, Texas. *Earth Surface Processes and Landforms*, *45*(3), 565–573. doi: 10.1002/esp.4754

Smith, V. B., & Mohrig, D. (2017). Geomorphic signature of a dammed sandy river: The lower Trinity River downstream of Livingston Dam in Texas, USA. *Geomorphology*, *297*, 122–136. doi: 10.1016/j.geomorph.2017.09.015

Tockner, K., Pennetzdorfer, D., Reiner, N., Schiemer, F., & Ward, J. V. (1999). Hydrological connectivity, and the exchange of organic matter and nutrients in a dynamic river–floodplain system (Danube, Austria). *Freshwater Biology*, *41*(3), 521–535. doi: 10.1046/j.1365-2427.1999.00399.x

Trigg, M. A., Bates, P. D., Wilson, M. D., Schumann, G., & Baugh, C. (2012). Floodplain channel morphology and networks of the middle Amazon River. *Water Resources Research*, *48*. (W10504) doi: 10.1029/2012WR011888

Verhoeven, J. T. A., Whigham, D. F., van Logtestijn, R., & O'Neill, J. (2001). A comparative study of nitrogen and phosphorus cycling in tidal and non-tidal riverine wetlands. *Wetlands*, *21*(2), 210–222. doi: 10.1672/0277-5212(2001)021[0210:ACSONA]2.0.CO;2

Ward, J. V., Tockner, K., & Schiemer, F. (1999). Biodiversity of floodplain river ecosystems: Ecotones and connectivity. *Regulated Rivers: Research and Management*, *15*, 125-139.

Wolf, K. L., Noe, G. B., & Ahn, C. (2013). Hydrologic connectivity to streams increases nitrogen and phosphorus inputs and cycling in soils of created and natural floodplain wetlands. *Journal of Environmental Quality*, *42*(4), 1245–1255. doi: 10.2134/jeq2012.0466